Review

Advances in Synthesis and Applications of Bismuth Vanadate Based Structures

Dragana Marinkovic *, Giancarlo C. Righini, Maurizio Ferrari *

Posted Date: 10 July 2025

doi: 10.20944/preprints202507.0958.v1

Keywords: bismuth vanadate; tetragonal structure; monoclinic structure; photocatalytic properties; degradation organic pollutants; water splitting; photoanode; photoelectrochemical (PEC) sensor; antimicrobial properties; food industry

 doi:10.20944/preprints202507.0958.v1

Review

Advances in Synthesis and Applications of Bismuth Vanadate Based Structures

Dragana Marinković [1,*], Giancarlo C. Righini [2] and Maurizio Ferrari [3]

[1] Vinča Institute of Nuclear Sciences, National Institute of the Republic of Serbia, University of Belgrade, P. O. Box 522, 11001 Belgrade, Serbia; draganaj@vin.bg.ac.rs (D.M), https://orcid.org/0000-0002-6017-2109

[2] Nello Carrara Institute of Applied Physics (IFAC CNR), Sesto Fiorentino, Firenze, 50019, Italy; righini@ifac.cnr.it (G.C.R.), https://orcid.org/0000-0002-6081-6971

[3] Institute of Photonics and Nanotechnologies (IFN CNR, CSMFO Lab.) and FBK Photonics Unit, Via alla Cascata 56/C, Povo, Trento, 38123, Italy; mferrari@fbk.eu (M.F.), https://orcid.org/0000-0003-3723-5957

* Correspondence: draganaj@vin.bg.ac.rs (D.M)

Abstract

In recent years, researchers have made great efforts to develop effective semiconductor photocatalysts to harness the visible spectrum of sunlight in photocatalytic applications. Bismuth vanadate, $BiVO_4$, has emerged as one of the most promising candidates for photocatalytic applications among few non-titania based visible light driven semiconductor photocatalysts. The $BiVO_4$-based structures are intensively studied due to their exceptional ionic conductivity, photocatalytic behavior under ultra-violet and visible light, dielectric properties, ferroelastic and paraelastic phase transitions, and strong pigmentation. $BiVO_4$ occurs in nature in three crystalline structures: orthorhombic pucherite, tetragonal dreyerite (tz), and monoclinic clinobisvanite (ms). All three crystal structures of $BiVO_4$ are n-type semiconductors with corresponding energy gap values of 2.34, 2.40 and 2.90 eV, respectively. Different methods of synthesis have been reported for preparation of $BiVO_4$ structures of varying morphologies and sizes. The morphology of $BiVO_4$ is strongly influenced by the preparation method and reaction parameters. A comprehensive systematic study of developments, preparation methods, structure, different properties and advances in different applications over the past decade in research on $BiVO_4$ based structure will be described. Finally, the current challenges and future outlook of the $BiVO_4$ based structure will be highlighted, in the hope of contributing to guidelines for the future applications.

Keywords: bismuth vanadate; tetragonal structure; monoclinic structure; photocatalytic properties; degradation organic pollutants; water splitting; photoanode; photoelectrochemical (PEC) sensor; antimicrobial properties; food industry

1. Introduction

Water pollution is one of the most serious of all environmental problems with critical effects on the human live. Photocatalytic degradation technology, including advanced oxidation processes (AOPs), has become increasingly more useful and necessary in the past few decades due to degradation a wide range of organic and inorganic contaminants. Obtaining photocatalysts with ideal performances is the core problem for photocatalysis [1, 2].

In recent decades, an immense research attention has been focused on solving the pollution problem and developing different kinds of semiconductor photocatalysts. A series of photocatalysts have been designed for this purpose. Since the traditional photocatalyst TiO_2 is limited in ultraviolet (UV) range applications, alternative materials have been widely explored. Owing to their unique properties, Bi-based semiconductor photocatalytic materials have been widely studied [2]. Among of different materials with photocatalytic properties, bismuth-vanadate ($BiVO_4$) showed great

 doi:10.20944/preprints202507.0958.v1

photocatalytic features to extend beyond the UV region due to its suitable band-gap of 2.4 eV and favorable band edge alignment to water splitting. $BiVO_4$ shows interesting physicochemical and dielectric properties, ferroelelasticity, semiconductivity, pigmentation, and photocatalytic features. $BiVO_4$ is polymorphous and occurs in three forms which can be prepared synthetically; scheelite-type structure with monoclinic (ms-) and tetragonal (ts-) systems, and zircon-type structure with tetragonal system (tz-). All three crystalline phases, *ts*-$BiVO_4$, *ms*-$BiVO_4$ and *tz*-$BiVO_4$, are n-type semiconductors with band gap energies of 2.34, 2.40, and 2.90 eV, respectively. A fourth form, i.e., an orthorhombic structure of $BiVO_4$, only occurs naturally as the mineral pucherite. As one of the promising non-titania (TiO_2) visible-light-driven photocatalysts, ms-$BiVO_4$ is studied intensively and there are many ways to prepare ms-$BiVO_4$ micro- and nanoparticles of varying morphologies and sizes. Also, due to yellow color, non-toxic ms-$BiVO_4$ is a good commercially available substitute to toxic cadmium- and lead-based yellow pigments [3, 4]. Following the work of Kudo's group in 1998 on photocatalytic evolution of O_2 under visible light irradiation of $BiVO_4$ in aqueous $AgNO_3$ solution [5-7], considerable research efforts have been devoted to the $BiVO_4$-based material. This material is an excellent candidate for use in photocatalytic water splitting and photocatalytic degradation of air/water pollutants [8, 9]. The *ms*-$BiVO_4$ is known to exhibit excellent photocatalytic activity under visible light; on the other hand, pure tz-$BiVO_4$ has been studied to a much lesser extent as a photocatalyst [10-12].

In order to improve the photocatalytic performance of $BiVO_4$, promoting the separation and transfer of photogenerated carriers, namely, the photoinduced electron (e^-) and hole (h^+) pairs, is necessary [13, 14]. There are a lot of $BiVO_4$-based heterojunction photocatalysts including: n-$BiVO_4$@p-MoS_2 [15], $CaFe_2O_4$/$BiVO_4$ [16], TiO_2/$BiVO_4$ [17, 18], rGO/$BiVO_4$ [19], Bi_2WO_6/$BiVO_4$ [20], Co_3O_4/$BiVO_4$ [21], $BiVO_4$/$Bi_4V_2O_{11}$ [22], Ag_3PO_4/$BiVO_4$ [23], $Cu_3Mo_2O_9$/$BiVO_4$ [24], $BiVO_4$/CdS [25], Bi_2S_3/$BiVO_4$/$MgIn_2S_4$ [26] and 2D Zn-MOF/$BiVO_4$ [27], which have been developed for photocatalytic decomposition of water, degradation of organic pollutants, reduction of CO_2 and heavy metal ions [28-30]. Enhanced photocatalytic performance has been reported for numerous doped $BiVO_4$ materials with zircon-type structure. Bi^{3+}-based compounds can be easily doped with rare ions (RE^{3+}) due to the equal valence and similar ionic radius. This means that RE^{3+} ions could be regarded as active co-catalysts and dopants in order to enhance the photocatalytic activity of $BiVO_4$ [31-33]. Also, other dopants like of Cu^{2+}, Yb^{3+}, Er^{3+}, Nd^{3+} and Sm^{3+} ions can induce modification of the $BiVO_4$ shape, increase of its active area and change drastically optical properties., while molybdenum (VI), Mo^{6+} and tungsten (VI), W^{6+}, can improve the electrical characteristics, the electron mobility and electrical conductivity of the $BiVO_4$ [34-39].

This review will be focused on the state of art of the basic and applied research on $BiVO_4$-based structures. A comprehensive systematic study of developments, preparation methods, structure, properties and advances in everyday applications over the past decades in research on $BiVO_4$-based structures will be described.

2. Discussion

2.1. Advances in Synthesis of $BiVO_4$-Based Structures

Different methods of synthesis have been reported for preparation of monoclinic *ms*-$BiVO_4$ or *tz*-$BiVO_4$ with various morphologies and sizes. Several approaches have been used: co-precipitation and micro-emulsion [40-48], hydrothermal synthesis with and without employing surfactant or template [49-56], rapid microwave-assisted process and microwave-assisted hydrothermal method [57-64] and solvothermal approach [65-71]. Using a precipitation method, the $BiVO_4$ can be obtained from an aqueous solution of NH_4VO_3 and an aqueous nitric acid solution of $Bi(NO_3)_3$ [58, 72-75] or from an aqueous nitric acid solution of Bi_2O_3 and V_2O_5 [12, 76]. By using microwave-assisted or hydrothermal technique, either an aqueous $NaVO_3$ or NH_4VO_3 solution with nitric acid of $Bi(NO_3)_3$ solution or Bi_2O_3 and V_2O_5 in a molar ratio in HNO_3 were mixed [77-82].

Several specialized methods have also been developed for the synthesis of $BiVO_4$. These include: (i) a reaction involving layered potassium vanadate powders (KV_3O_8 and $K_3V_5O_{14}$) and $Bi(NO_3)_3$ in aqueous solution, using a controlled vanadium-to-bismuth ratio [83]; (ii) a high-temperature colloidal synthesis in which $Bi(NO_3)_3$, NH_4VO_3, and polyethylene glycol (PEG) are

 doi:10.20944/preprints202507.0958.v1

dissolved in water [84]; and (iii) a low-temperature molten salt method employing a $LiNO_3$–$NaNO_3$ eutectic mixture (heated to 200 °C) as the solvent and a $BiVO_4$ precursor, obtained as a precipitate from $Bi(NO_3)_3$ and NH_4VO_3 solutions, as the solute.[85]. Structural phase transition in $BiVO_4$ (from monoclinic to tetragonal) can occurs under high pressure [86, 87].

The $Bi(NO_3)_3x5H_2O$ was used in most syntheses of the $BiVO_4$ as a bismuth precursor owing to its wide availability and cheapness. However, $Bi(NO_3)_3x5H_2O$ readily hydrolyzes into basic salts, $BiO(NO_3)$ and $Bi(OH)_2NO_3$, and other nitrates with numerous complicated compositions [88, 89]. Recently, a novel and non-conventional way of synthesis was attempted, through a straightforward room-temperature non aqueous preparation method for producing nanocrystalline tz-$BiVO_4$: NH_4VO_3 and $Bi(NO_3)_3{\cdot}5H_2O$ have been employed as precursors, with ethylene glycol serving as both the solvent and reaction medium for precipitation. Additionally, it functions as a capping agent, limiting particle growth and preventing agglomeration [90–92].

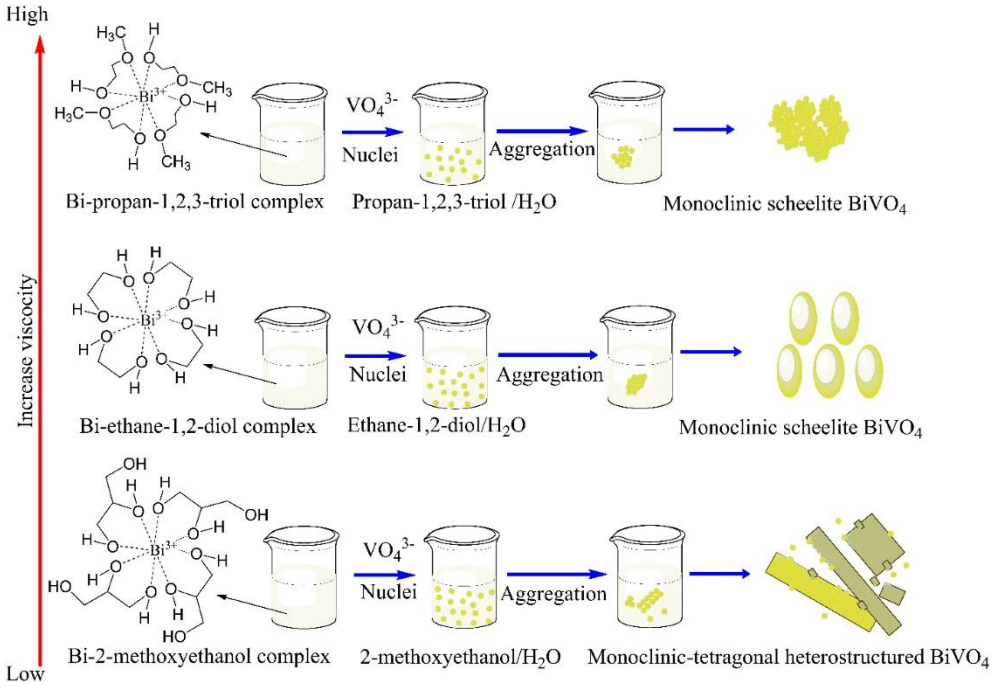

Figure 1. The formation mechanism of $BiVO_4$ samples prepared using mixed solvents. The image was adapted from the reference [93], with permission of Elsevier.

The Figure 1 schematically illustrates the formation process of the monoclinic/tetragonal $BiVO_4$ heterostructure (m–t $BiVO_4$), which involves nucleation followed by aggregation-driven growth. The phase transition from the monoclinic to the tetragonal structure is attributed to the stability of the MEOH–Bi complex formed during solvothermal treatment. In this process, Bi^{3+} ions coordinate with both the oxygen atom of the C–O–C bond and that of the O–H bond in the 2-methoxyethanol (MEOH) molecule. Notably, the relative intensity of the (200) diffraction peak, associated with the tetragonal phase, increases with prolonged thermal treatment [93].

2.2. Advances in Morphologies and Sizes of $BiVO_4$-Based Structures

The morphology of $BiVO_4$ material has a significant impact on the photocatalytic efficiency and other applications. The final morphology of $BiVO_4$ particle is strongly influenced by the preparation method and reaction parameters such as concentration and pH of precursor solution, solvent, reaction temperature, duration, molar ratio of Bi^{3+}/V^{5+}, surfactant and dopant. The morphology of $BiVO_4$ as photocatalysts significantly enhances the performance of ceramic membranes in oily wastewater treatment [94]. The initial pH of the precursor solution is found to be a critical parameter in defining the phase and final morphology of $BiVO_4$ particles [95-99]. The $BiVO_4$ samples prepared by different methods of synthesis have different morphologies and size, such as: i) highly uniform

 doi:10.20944/preprints202507.0958.v1

monodisperse nanospheres of 125 nm in diameter [100]; ii) irregular spheres (20-100 nm or few micrometers) [101,102]; iii) hollow spheres (~700 nm) [103, 104]; iv) nanorods (length of 300 nm) [105, 106]. Other $BiVO_4$ particles with unusual morphologies have been realized, like: needle (50-400 nm) and irregular dog-bone (300-600 nm) [107], butterfly (4-10 μm) [108], leaf peanut (1 – 10 μm) and roundish aggregates (1 – 5 μm) [109-111], polyhedral (6 – 8 μm) [112, 113], decagonal shape rods (2–3 μm) [114], potato and broccoli-like (150 - 500 nm) [115], bowknot (5μm) and dumbbell-like (~3 μm) [116]. Additionally, there are several publications about tz-$BiVO_4$ spherical nanoparticles with diameters in a range of 10-40 nm and ellipsoidal shape with the radius of about 20 nm [58, 117]. Compared to larger particles or bulk material, nanostructured materials with larger surface areas showed a significantly enhanced reactivity and higher photocatalytic activities for water splitting under UV light irradiation [118, 119].

Field emission scanning electron microscopy (FESEM) technique was generally used to observe the morphologies of $BiVO_4$ samples. Figures 2a) and 2b) show the prepared $BiVO_4$ samples like microspheres and dumbbell-like, according to the use of different molecular weight of PEG in the synthesis. The results indicated that $BiVO_4$ with different microstructures can be selectively synthesized by simply changing the molecular weight of PEG. Also, the morphologies of samples can be controlled through varying the pH value of hydrothermal process, to get as spindle and wheat like $BiVO_4$ samples, as shown in Figures 2c) and 2d) [116].

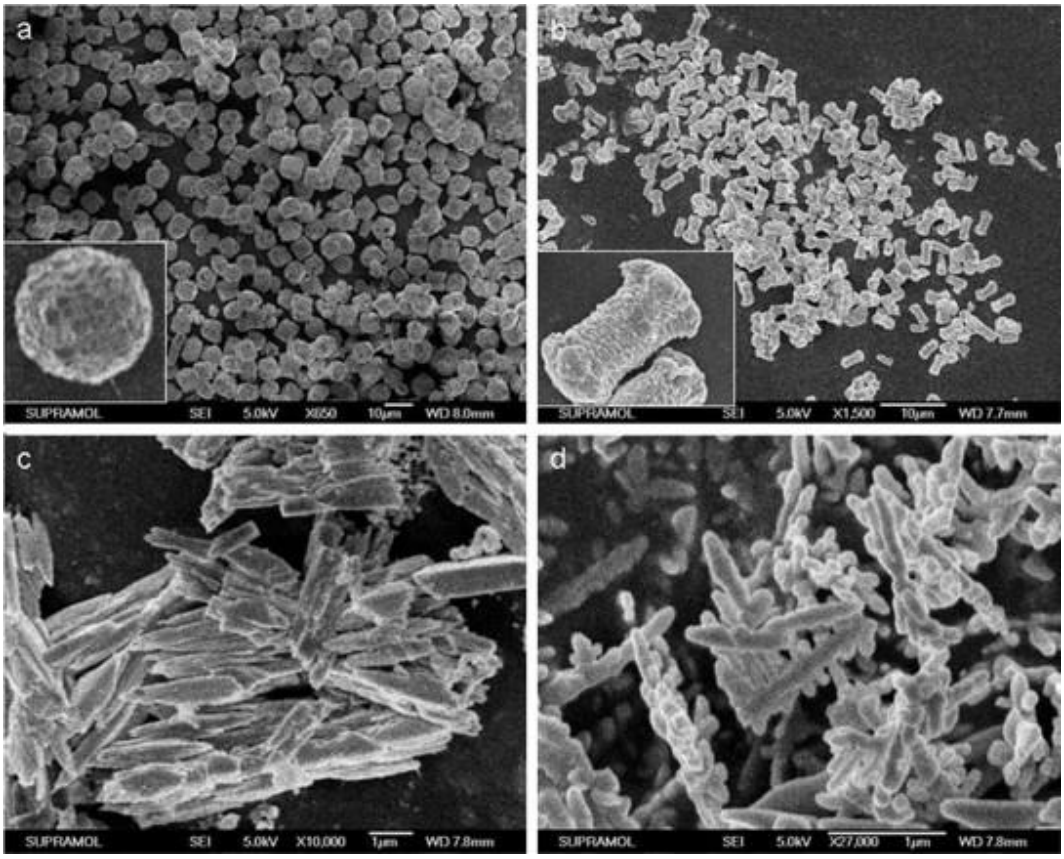

Figure 2. FESEM images of the as-prepared $BiVO_4$ samples: a) spherical sample, b) dumbbell like sample, c) spindle like sample and d) wheat like sample. Figure reproduced with modifications from the reference [116], with permission of Elsevier.

The scanning electron microscopy (SEM) images of the $BiVO_4$ samples with different morphologies obtained for various Bi^{3+}/V^{5+} molar ratios are shown in Figure 3. When the Bi^{3+}/V^{5+} molar ratio is 1.0, micrometer-sized dumbbells (constructed from the assembly of many nanorods) with length of about 4–7 μm appear (Figures 3a and 3b), while when the Bi^{3+}/V^{5+} molar ratio is 0.77, the obtained samples are composed of microrods with average diameter of about 1.4 μm (Figures 3c and 3d). As the molar ratio is reduced to 0.67 and 0.56, the $BiVO_4$ ellipsoids with diameter of 1.0–1.3 μm and length of 1.5–2.0 μm, consisting of many small nanoparticles, and microspheres with an

 doi:10.20944/preprints202507.0958.v1

average diameter of 1.1 μm are obtained, respectively (Figures 3e – 3h). As the Bi^{3+}/V^{5+} molar ratio is adjusted to 0.5, the $BiVO_4$ particles with cake-like morphology, constituted by many small nanoparticles, and uniform size about 1.1 μm are formed (Figures 3k and 3l). In order to obtain detailed information on the structure and morphologies of as-synthesized samples, transmission electron microscopy (TEM) additionally can be performed.

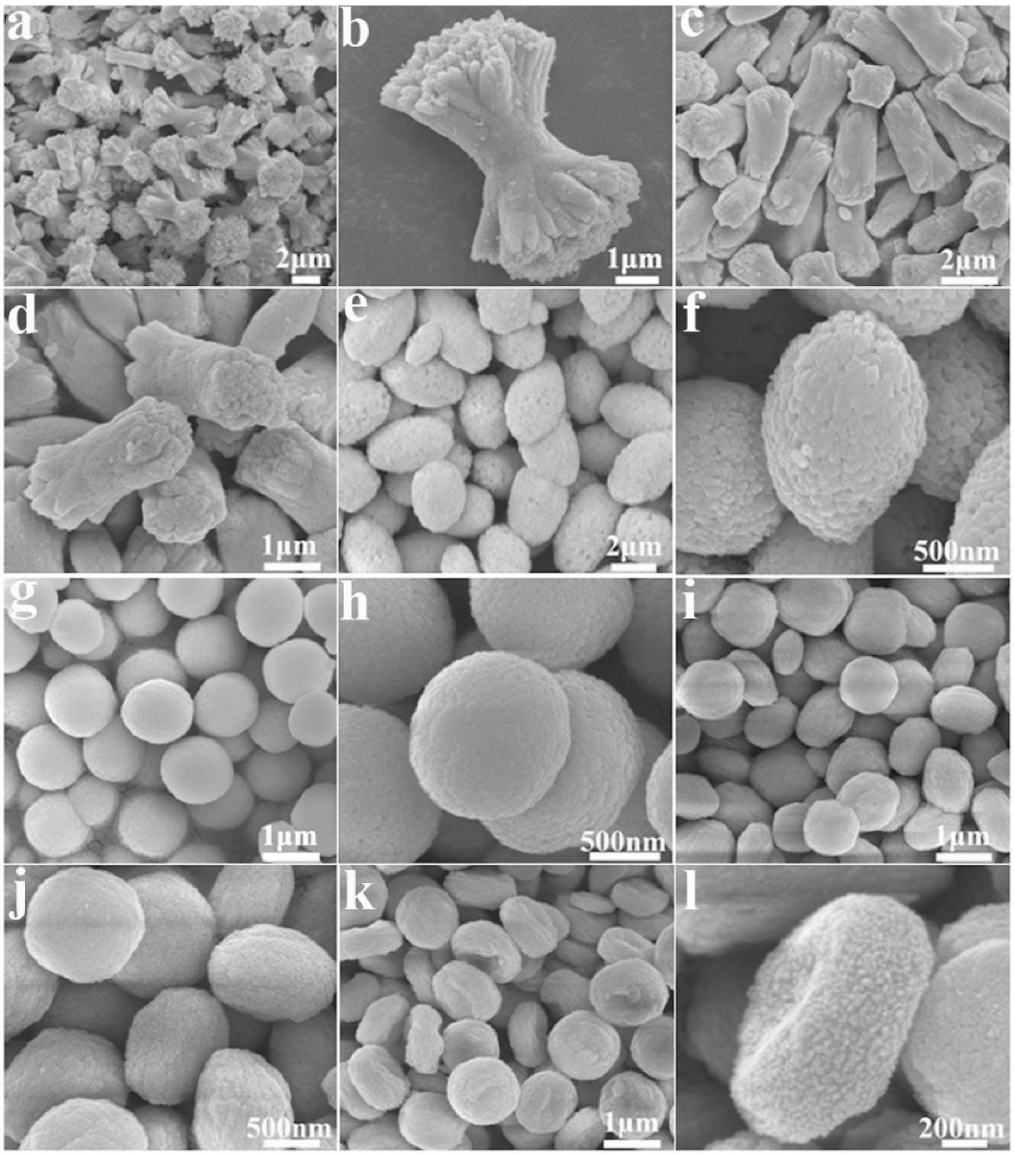

Figure 3. SEM images of $BiVO_4$ samples with different Bi^{3+}/V^{5+} molar ratios: a), b) 1.0, c), d) 0.77, e), f) 0.67, g), h)) 0.56, i), j) 0.50 and k),l) 0.40. The figure was adapted from the reference [120], with permission of Elsevier.

2.3. Crystal and Electronic Structure of $BiVO_4$

This section discusses various crystal structures and the electronic structure of $BiVO_4$ related to photo-electrochemical properties. $BiVO_4$ is an n-type semiconductor and can be synthesized in three crystal phases: monoclinic-scheelite (ms), tetragonal-zircon (tz), and tetragonal-scheelite (ts), as mentioned before and shown in Figure 4. The natural structure of $BiVO_4$ as a mineral is pucherite with the orthorhombic crystal, and this structure cannot be obtained in laboratory [121, 122]. The scheelite structure has a tetragonal crystal system (space group: I41/a where a = b = 5.1470, c = 11.7216 Å) or a monoclinic crystal system (space group: I2/b with a=5.1935, b = 5.0898, c = 11.6972 Å, and β= 90.3871°) [123] whereas the zircon-type structure consists of a tetragonal crystal system (space group: I41/amd with a = b = 7.303 and c = 6.584 Å). In the $BiVO_4$ scheelite structure, each Bi atom, similar as Gd^{3+} in $GdVO_4$ matrix, [123] is coordinated by eight oxygen atoms from different VO_4 tetrahedral units and each V atom is coordinated by four oxygen atoms at the tetrahedral site [124], as shown in

 doi:10.20944/preprints202507.0958.v1

Figure 4a and 4b, where Bi and V centers are coordinated along the [001] direction. Each oxygen atom is coordinated by two Bi and one V centers, forming a three-dimensional network bridging Bi and V centers together. However, monoclinic scheelite structure shows differences such as more distortion in the local environment of Bi and V ions, two different V–O bond lengths (1.69 and 1.76 Å) and four different Bi-O bond lengths (2.35, 2.37,2.52 and 2.63 Å) that lead to loss of four-fold symmetry [124]. Whereas for tetragonal scheelite structure, all four V-O bond lengths are equal to 1.73 Å, two different bond lengths Bi-O (2.4 and 2.47 Å) exist [124]. The observed significant distortion in the monoclinic scheelite structure enhances the local polarization leading to better electrons and holes separation and superior photo-electrocatalytic activity compared to tetragonal scheelite structure [125]. The local environment of Bi and V centers for zircon-type structure is shown in Figure 4, where eight oxygen atoms coordinate Bi by six different VO_4 tetrahedral units because two VO_4 tetrahedral units provide two oxygen atoms to Bi atom. Each V atom is coordinated by four oxygen atoms [126].

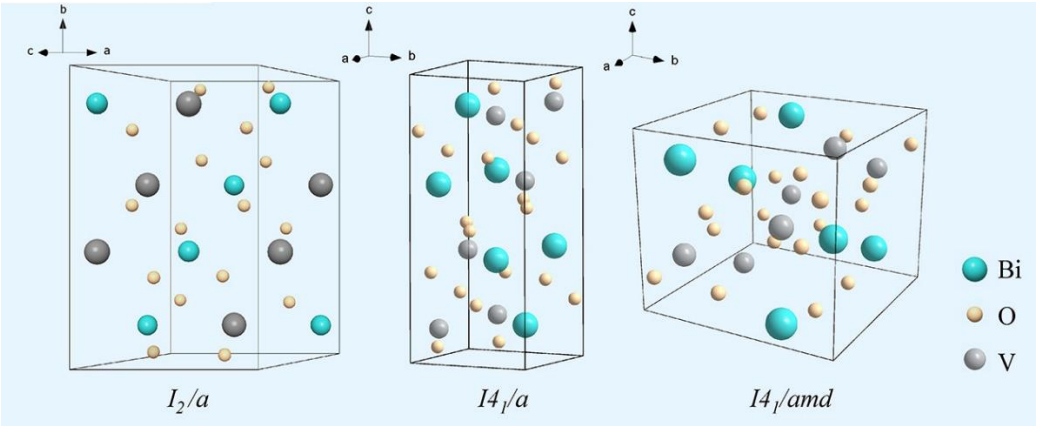

Figure 4. Graphic illustration of three crystal structures in $BiVO_4$: monoclinic scheelite (I_2/a), tetragonal scheelite ($I4_1/a$) and zircon-type tetragonal ($I4_1/amd$), respectively. The figure was adapted from the reference *[86]*, with permission of American Chemical Society.

The band gap energy of $BiVO_4$ allows it to be active in the visible region, with values of 2.4 eV for the scheelite structure and 2.9 eV for the zircon type structure. $BiVO_4$ does not yet attain practical conversion efficiency. The most limiting factor for $BiVO_4$ conversion efficiency is the fast recombination of photogenerated electron-hole pairs [127-133]. The density functional theory (DFT) calculations indicated changes in bandgap and density of states and showed that the smaller band gap of monoclinic bismuth vanadate, compared with the zircon type, is coming from hybridization between the Bi 6s state and the O 2p states at the top of valence band [134]. The conduction band is primarily composed by V 3d states, with additional contribution of O 2p and Bi 6p orbitales [135]. The coupling of states results in an upward dispersion of the valence band, and a lowering of the conduction band to a minimum, causing symmetric electron and hole masses, which facilitate a relatively efficient charge carrier separation and extraction [136]. The first-principles band structure calculations demonstrate the direct character of the $BiVO_4$ band gap [90-92].

3. Advances in Applications of $BiVO_4$-Based Structures

3.1. Degradation of Organic Compounds: Role of $BiVO_4$ Based Composites Photocatalysts

This section discusses the degradation of various organic compounds in the presence of the $BiVO_4$-based structures and composites photocatalysts. In recent years, researchers have been making great efforts to develop effective semiconductor photocatalysts to harness the visible spectrum of sunlight in photocatalytic applications. A method for the degradation of toxic organic compounds/pollutants from environment using semiconducting materials is an attractive approach. Nano-sized ball-like structure of $BiVO_4$ nanoparticles can act as a good photocatalyst, sensor and heavy metal detector. Photocatalytic efficiency was assessed through degradation studies using methylene blue (MB) dye under visible light irradiation, demonstrating an impressive 93% degradation rate [82, 137, 138]. In the case of the $BiVO_4$/graphene nanocomposite, effectively

 doi:10.20944/preprints202507.0958.v1

degradation of methyl orange (MO) was spotted while the photocatalytic activity increased, resulting in different composites, after excitation of $BiVO_4$ photocatalyst and generation of the electron–hole pairs [139]. On another side, the $BiVO_4$@MWCNT photocatalysts were synthesized by incorporation of the synthesized $BiVO_4$ nanoparticles with various percentages of multi-walled carbon nanotube (MWCNT) and were used as probes for the photocatalytic removal of atrazine (AZ) under visible light illumination [140]. The p-n heterojunction photocatalyst prepared by decorating CuO micro-planks with spherically shaped $BiVO_4$ was proved to be efficient in degradation MB and Cr(VI) reduction under visible light irradiation. Moreover, two-dimensional (2D) TiO_2 aerogel powder decorated with $BiVO_4$ (TiO_2/$BiVO_4$) was used for reduction of toxic Cr(VI) to Cr(III) [141, 142]. The Bi/$BiVO_4$ microstructures with novel hollow chainlike morphology were successfully fabricated. Owing to the synergistic interaction between them, improved photocatalytic activity was observed for photodegradation of Rhodamine B (RhB) under visible-light illumination, compared to the $BiVO_4$ and Bi photocatalytic single action. [143]. The synergistic effects of oxygen vacancies and built-in electric fields in $GdCrO_3$/$BiVO_4$ and 2D/2D $InVO_4$/$BiVO_4$ heterostructures effectively enhanced their photocatalytic performance for nitrate reduction in water and improved their photoelectrochemical activity, respectively, by facilitating charge separation and suppressing recombination [144, 145].

Pharmaceuticals and antibiotics have been classified as critical water pollutants. In order to find a suitable technique for removing them from contaminated water, the photoelectrocatalytic oxidation method has attracted much attention in recent years. The $BiVO_4$/Ag_2S p-n heterojunction fabricated by using electrodeposition and successive ionic layer adsorption on fluorine-doped tin oxide glass (FTO) or graphitic carbon nitride (g-C_3N_4) decorated with Pt@$BiVO_4$ have been used for degradation of ciprofloxacin and sulfamethoxazole [146, 147].

Figure 5 shows the UV–visible absorption peak spectra related to the degradation of MB dye in 24 hours, as a function of the magnetic stirring rotation speed.

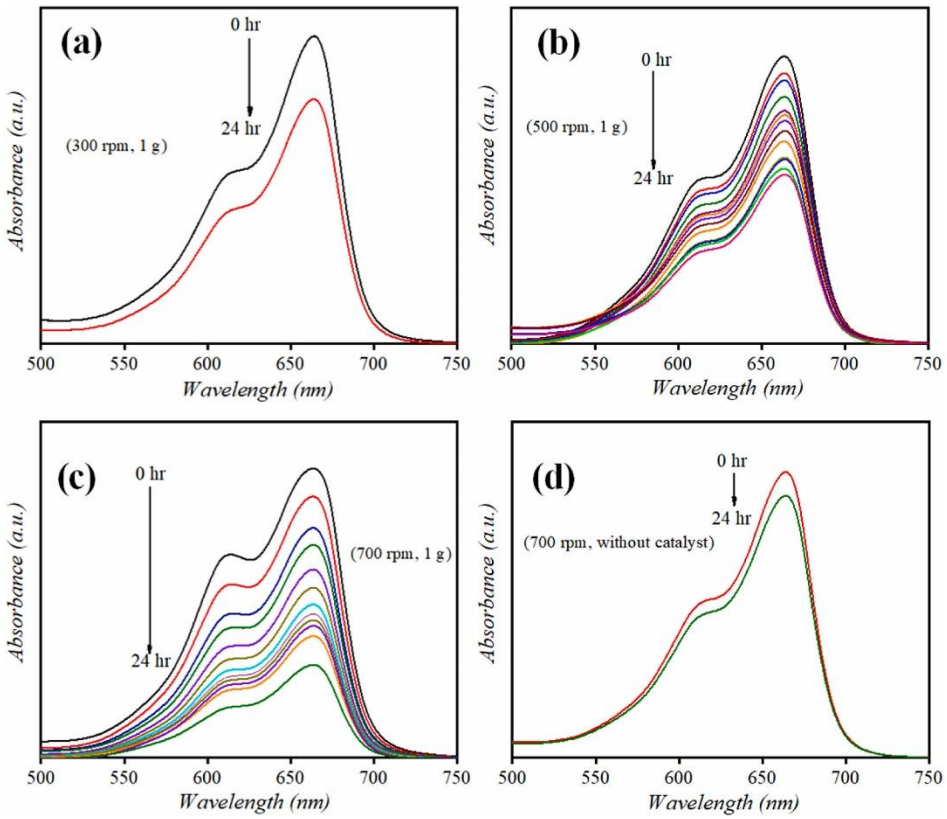

Figure 5. Absorbance spectra of MB dye in 24 hours using 1 g of $BiVO_4$ at different at rotational speeds: (a) 300 rpm, (b) 500 rpm, (c) 700 rpm, and (d) without any catalytic dose (control) at 700 rpm. The Figure was adapted from the reference [148], with permission of Elsevier.

 doi:10.20944/preprints202507.0958.v1

The degradation rate efficiency (D) can be calculated using Eq. (1). The degradation of dye catalyzed by $BiVO_4$ is analyzed using the pseudo-first-order kinetics model (Eq. (2)), and the rate constant of dye degradation is calculated [149].

$$D(\%) = \frac{Co - Ct}{Co} \times 100 \quad \text{Eq. (1)}$$

$$-ln\left(\frac{Ct}{Co}\right) = Kt \times t \quad \text{Eq. (2)}$$

where C_0 is the initial solute concentration, Ct is the solute concentration at a certain reaction time (t), and k is the pseudo-first-order rate constant.

On other side, the sonocatalysis activity of $BiVO_4/FeVO_4$ composites was investigated by analyzing the removal process of the drug model tetracycline (TETR). In comparation to $BiVO_4$, the composites exhibited significantly enhanced sonocatalytic activity in degrading TETR due to the formation of type-II heterojunctions, which promoted the effective electron-hole pairs separation [150].

3.2. Antimicrobial Activity of the $BiVO_4$-Based Structures

$BiVO_4$ has also been studied as potential non-toxic material for biomedical applications due to its antibacterial activity against various pathogenic bacteria. The antibacterial activity of this material was estimated by using pathogenic microbes Escherichia coli (E. coli) and Staphylococcus aureus (S. aureus) [151]. The photo-induced high antimicrobial activity of monoclinic-$BiVO_4$ nanoparticles has also been tested in antimicrobial efficiency and environmental remediation applications based on its photocatalytic activity targeting organic dyes and different water pollution [152]. The $BiVO_4$@activated carbon fiber can be used as antibacterial agent against both E. coli and S. aureus with enhanced recyclability [153]. Antibacterial efficacy was assessed against by Gram-positive (E. coli and S. aureus) and Gram-negative (E. coli and Pseudomonas aeruginosa) bacteria using $BiVO_4$ and Ta-doped $BiVO_4$ nanoparticles at various concentrations [154]. Bacterial cultures were incubated with Ta-$BiVO_4$ nanoparticles under visible light illumination and in dark for the antibacterial assays. The antimicrobial activity of Ta-doped $BiVO_4$ nanoparticles was successfully assessed indicating their potential as strong antimicrobial agents against both Gram-positive and Gram-negative bacteria [154-156]. Antimicrobial activity of $BiVO_4$ nanoparticles against six different bacterial strains is presented in Figure 6.

 doi:10.20944/preprints202507.0958.v1

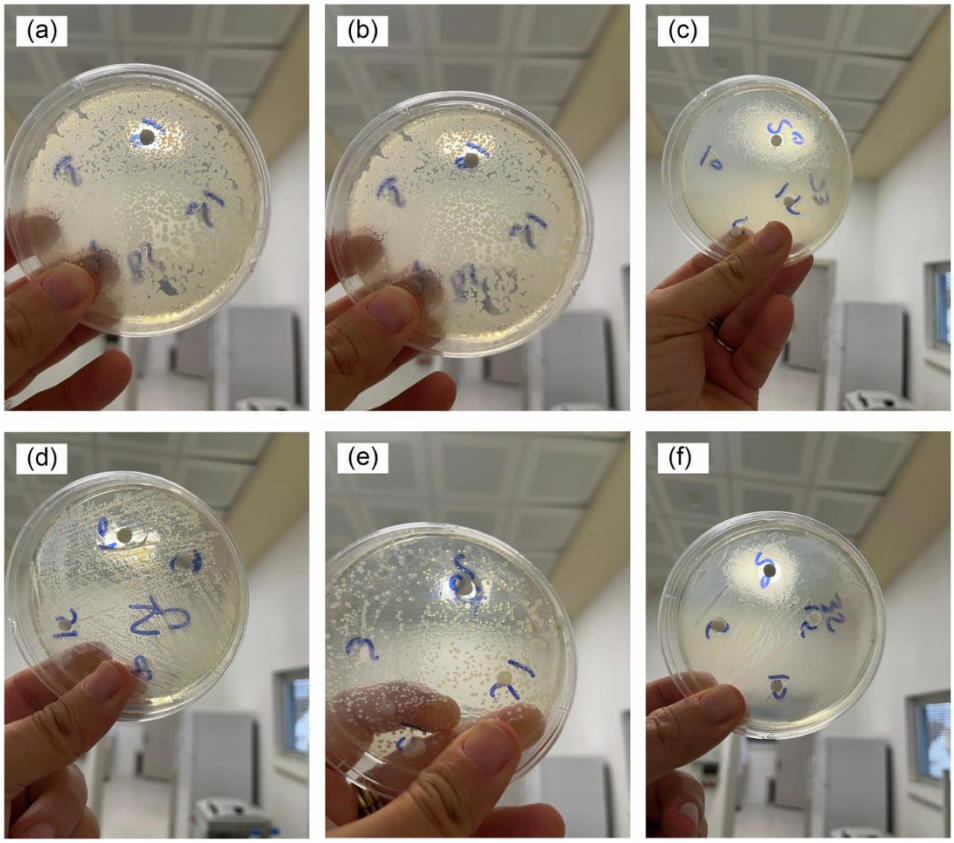

Figure 6. Antimicrobial activity of $BiVO_4$ nanoparticles against (a) B. subtilis, (b) B. cereus, (c) E. coli, (d) P. aeruginosa, (e) S. aureus and, (f) S. enteritidis**.** The figure was adapted from the reference [155] under a Creative Commons 4.0 License.

The antibacterial activity and the generation of reactive oxygen species (ROS) of $BiOCl/BiVO_4$ heterojunction can be improved compared to $BiVO_4$ [157]. The ROS produced in the PDA-rGO/$BiVO_4$ heterojunction blocked the transmembrane transport of bacteria, as confirmed by using ROS fluorescence detection [158]. The antibacterial and UV protection properties of the prepared $CuO/BiVO_4$@cotton were also studied. The $CuO/BiVO_4$ nanocomposite has overcome the low quantum efficiency of pure $BiVO_4$. The nanocomposite possesses very good recyclability of the photocatalyst on cotton fabrics/flexible textile with multiple functions beside degradation of pollutants from waste water [159]. The normal inactivated tested bacterial strains with a smooth surface attributed to the production of ROS species such as OH and O^{2-}, which easily cross the cell membrane and enter the interior of the strains [160, 161].

3.3. Application of the $BiVO_4$-Based Structures in Food Industry

The $BiVO_4$ is an ideal starting material for antioxidant surveillance under visible light irradiation. Due to unsatisfactory charge collection and utilization in practical applications, the $BiVO_4$ is usually doped to exploit the effects of dopants on the photocatalytic behavior under visible light illumination. The substitution of Bi^{3+} or V^{5+} ions with other M^{3+} or M^{6+} metal ions leads to significant changes in physical properties such as structural distortions of crystal unit, formation of a new phase, and to evident changes in morphological, optical and electrical properties due to the different ionic radii of the involved ions. This proof-of concept is useful in detection of antioxidant capacity in the foodstuff industry, opening up a bright future in cosmetic and healthcare areas [162]. A label-free photoelectrochemical (PEC) sensor based on $BiVO_4$@GO composites was prepared for detection of antioxidants and antioxidant capacity of food. Large surface area and good conductivity make the $BiVO_4$@GO composites an unique promising sensor for detection of antioxidant capacity in food, which will help the organism to take enough antioxidants to defend against free radicals [163], while the crystal-reconstructed $BiVO_4$ PEC biosensor can be applied in the fields of multi-tumor or viral biomarker detection [164]. The composition and pH of the electrolyte, applied bias, as well as surface

 doi:10.20944/preprints202507.0958.v1

morphology of the photoactive layer can have significantly effect on the selectivity and use of the PEC sensors [165]. The synthesized $BiVO_4$ PEC sensor with unique carnation-like morphology and high specific surface resulted in high possibility for Cr(VI) detection, with a wide linear range of 2–210 μM and a very low limit of detection (LOD) of 0.01 μM. This $BiVO_3$ based PEC sensor can be used, for instance, in food safety monitoring for Cr(VI) detection in peanuts, rice, soil and tap water, with satisfactory recovery rates of 90.3 to 103.0% [166].

Propyl gallate is widely used in the food industry as one of the most important additives to prevent the oxidation processes. The synthesized $Cu_3(PO_4)_2/BiVO_4$ composites and GCE/$BiVO_4$/ZrO_2@graphene electrode can be used for determination of propyl gallate and of acetaminophen, phenylephrine hydrochloride and cytosine, respectively, in different food products. These materials are beneficial for food quality monitoring and reduce the risk of propyl gallate overuse in food and are recommended for potential medical applications [167, 168]. A new photosensitive sensor was developed for the successful electrochemical analysis of quercetin from natural samples using ITO/MWCNT@PC@$BiVO_4$ composite due to the photosensitivity and stable structure of $BiVO_4$ high electron permeability of MWCNT and advantageously electron transfer [169, 170].

The synergic effects between g-C_3N_4 and $BiVO_4$ in the g-C_3N_4/$BiVO_4$ composites used as a photoactive material produced photocurrent signals resulting in an increased photocurrent response after the composites fix on the surface of the FTO electrode [171]. The illustration of g-C_3N_4/$BiVO_4$ PEC sensor for tetracycline (TC) residue detection in food samples (honey) and animal products (kidney, milk, pork) is presented on the Figure 7.

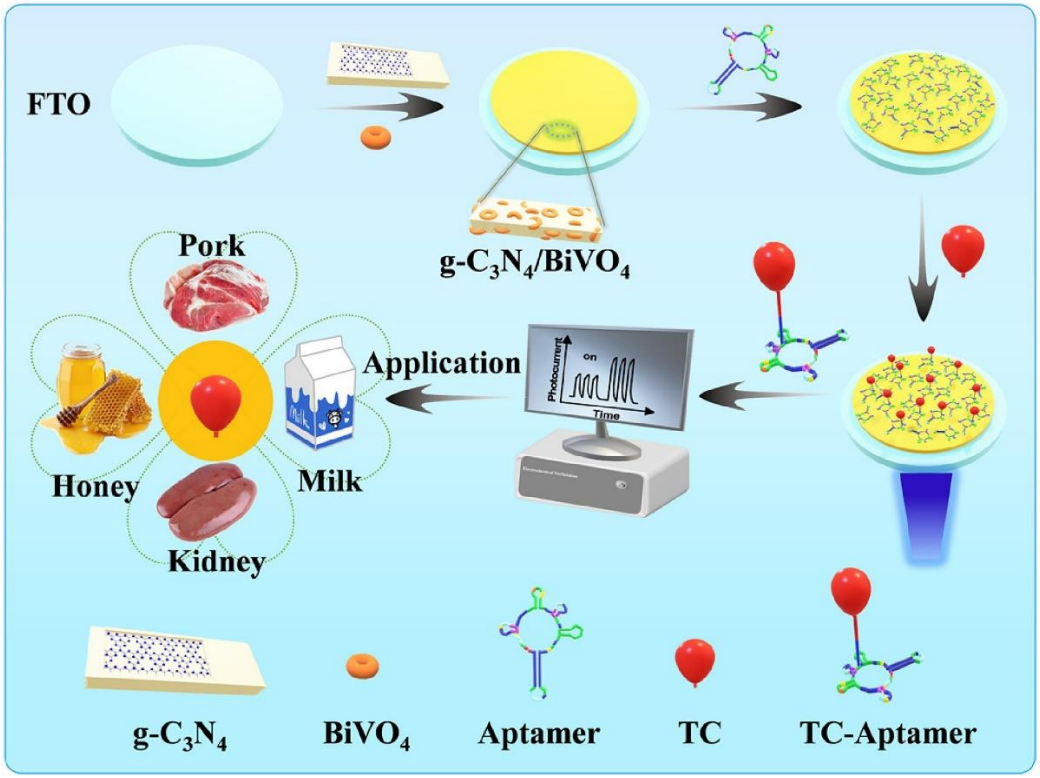

Figure 7. Schematic illustration of g-C_3N_4/$BiVO_4$ PEC sensor for tetracycline detection in food samples**.** Figure reproduced from the reference [171], with permission of Elsevier.

3.4. Applications of the $BiVO_4$-Based Structures as Photoelectrode in Water Splitting

In recent years, in addition to the application in the environmental protection of the $BiVO_4$-based structures for organic pollutant degradation, superior antimicrobial properties and food safety monitoring, attention has been also paid to the research focused on multipotential applications of these structures [172]. $BiVO_4$ -based photoelectrodes show great potential in several practical

 doi:10.20944/preprints202507.0958.v1

applications. Due to good visible light responsiveness and stable optoelectrical properties, the $BiVO_4$ -based structure can be widely used for efficient water splitting and hydrogen production [173, 174].

To fabricate photoanodes with large-area possessing excellent and uniform PEC activities, it is very important to include defect states of the material. Following this way, highly efficient $BiVO_4$ photoanodes containing adjustable concentrations of bismuth and oxygen vacancies, $Bi_{vac.}$ and O_{vac}, were fabricated [175]. With the aim to promote charge separation in the bulk material, the $BiVO_4$ based photoanode with lattice strain was prepared by generating Bi vacancies [176]. In addition, $BiVO_4$ photoanodes were also used in PEC cells for the production of various chemicals, as well as for PEC water splitting [177].

Water splitting based on numerous visible-light-responsive photocatalysts is one of the most important and cost-effective approaches for the conversion of solar energy into clean and renewable hydrogen energy and production of green H_2 on a large scale. This result can be easily achieved in a one-step excitation system using a single photocatalyst or Z-scheme strategies based on a pair of photocatalysts [178, 179]. Because photoelectrochemical water splitting techniques often require a corrosive electrolyte, limiting their stability and environmental sustainability, the alternatively way for clean production of hydrogen can be obtained directly from sunlight and water by photocatalytic water splitting [180].

The $BiVO_4$ material possesses several limitation parameters including low charge mobility, high bulk recombination rates and oxygen evolution reaction (OER) kinetics at the surface for its use as high-performance PEC photoanodes for solar water splitting. Numerous strategies have been applied to improve these performances and the texture engineering has emerged as a promising approach. One approach for improving the PEC efficiency is based on the controlling the crystallographic orientation and exposed facets which enhancing charge transport and reduce surface recombination [181]. Following this direction in preparation, the octadecahedral-$BiVO_4$ photoanodes was successfully produced with exposed {040}, {011} and high-reactivity {121} facets. It was shown the charge separation is dramatically improved and the {121} facets show better oxygen evolution reaction (OER) activity for triggering water oxidation than the {040} and {011} facets [182]. Other approaches for improving the PEC efficiency are based on different morphologies, doping, modification and making different $BiVO_4$-based composites. The $BiVO_4$ nanowires due to negative surface photovoltage signal are suitable for the construction of membranes for solar energy conversion [183]. A suitable doping concentration of Cu in $BiVO_4$ resulted in enhanced electronic conductivity and improved charge transfer dynamics compared to un-doped $BiVO_4$ [184, 185].

Multi-interfacial optimization of $BiVO_4$-based composites to improve charge separation efficiency due to synergistic effect within the material matrix has emerged as a main strategy for improving PEC performance [186]. Ti_3C_2 quantum dots-modified $BiVO_4$ photoelectrodes, $BiVO_4/Ti_3C_2$ QDs, for water splitting H_2 production, showed improved photoelectron-hole pairs separation and photocurrent density of about 2.5 times higher than that of bare $BiVO_4$ [187]. On other side, due to the synergistic effect of CuSCN and Ni: FeOOH, the photocurrent density of the optimized $BiVO_4$/CuSCN/Ni: FeOOH photoanode is 3.39 times higher than that of pure $BiVO_4$ [188]. Similar ratio in photocurrent density is obtained for photoanode $BiVO_4$/Co,Fe-NTMP (nitrilotris methylene phosphonic acid) and $BiVO_4$ [189]. The RGO@g-C_3N_4/$BiVO_4$ photocatalysts has dual applications in photo electrocatalytic H_2 production and antibiotics tetracycline chloride degradation. Triple composites of g-C_3N_4/RGO/$BiVO_4$, formed by the synergistic effect between $BiVO_4$, RGO and g-C_3N_4, show significant photocatalytic activity compared to pure $BiVO_4$ or g-C_3N_4 [190]. Recently, the Ag/$BiVO_4$ composite for application in H_2O_2 fuel cell was fabricated. Compared with $BiVO_4$ nanoplates, the Ag/$BiVO_4$ composite has a narrower band gap, enhanced visible light absorption and high photocatalytic activity and it provides a new strategy model for the efficient conversion and utilization of solar energy [191]. On other hand, 10 cm^2 perovskite-$BiVO_4$ tandem PEC devices were fabricated with a selective Cu92In8 alloy catalyst which could demonstrate syngas production coupled to O_2 evolution over 36 hours [192].

An example of the photocatalytic system based on the $BiVO_4$ composites is presented in the scheme shown in Figure 8. The system is composed of two separate reaction parts: a hydrogen evolution cell containing halide perovskite photocatalysts ($MoSe_2$-loaded $CH(NH_2)_2PbBr_{3-x}I_x$) and an

 doi:10.20944/preprints202507.0958.v1

oxygen evolution cell containing NiFe-layered double hydroxide modified $BiVO_4$ photocatalysts mediated by the I_3^-/ I^- redox shuttle [193].

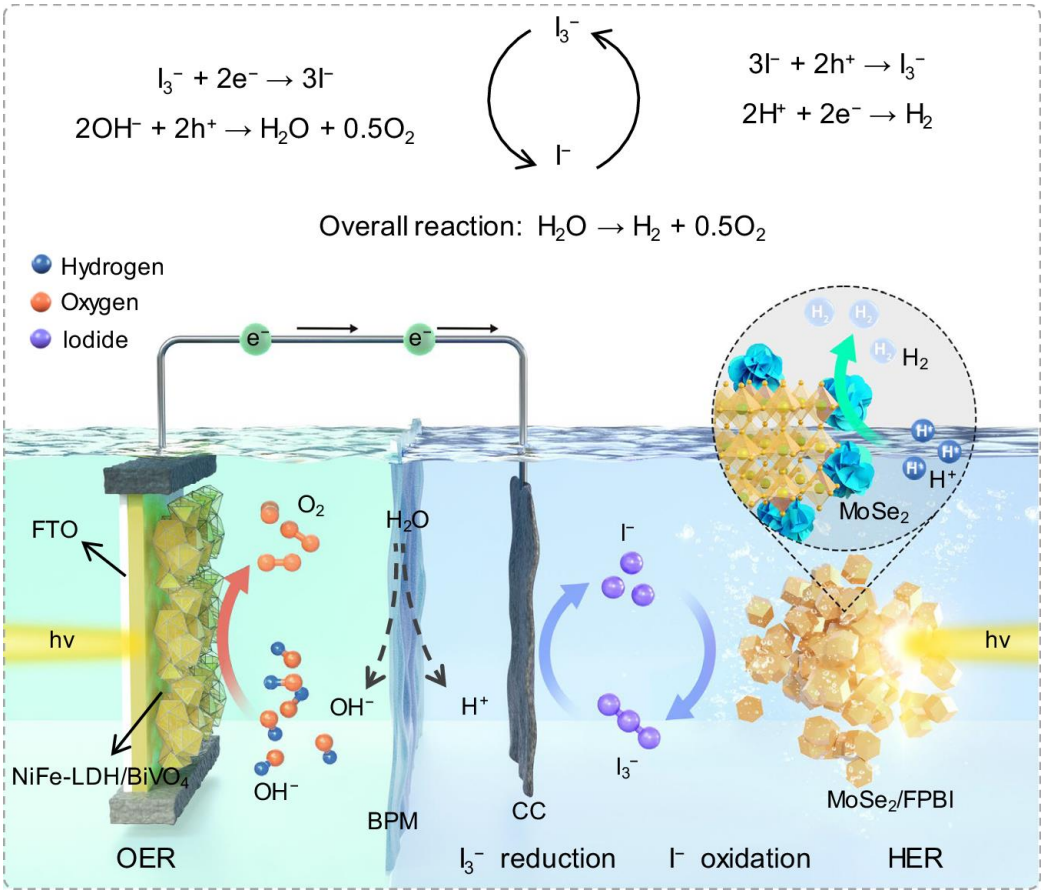

Figure 8. Schematic illustration of the Z-scheme solar water splitting system with separated H_2 and O_2 production. The net reaction is water splitting to produce H_2 and O_2 mediated by the I_3^-/I^- redox shuttle. (HER - hydrogen evolution reaction, OER - oxygen evolution reaction, NiFe-LDH/$BiVO_4$ I− I_3^- I^- oxidation H_2 $MoSe_2$ H^+ $MoSe_2$/FPBI HER hν represents NiFe layered double hydroxide modified $BiVO_4$. FPBI/$MoSe_2$ represents $FAPbBr_{3-x}I_x$ (FPBI, $FA=CH(NH_2)_2^+$) loaded with molybdenum selenide, CC-carbon cloth and FTO - fluorine-doped tin oxide coated glass). **The f**igure is reproduced from the reference [193]. Under Creative Commons 4.0 License.

4. Conclusions

This review has provided a systematic study and a related bibliography concerning developments, preparation methods, structures, different properties applications and recent advances of the research on $BiVO_4$-based structure. Additionally, a detailed discussion was given regarding the preparation approaches, processes, morphology, crystal and electronic structure, performance, and application perspective of these materials. A method of degradation of toxic organic compounds/pollutants in the environment using semiconducting materials is a very attractive approach. Photodegradation of various organic compounds methylene blue, Rhodamine B, atrazine, as well as pharmaceutical species, such as ciprofloxacin and sulfamethoxazole, in the presence of the $BiVO_4$-based photocatalysts under visible light irradiation was explained in detail. $BiVO_4$ has been studied as the non-toxic material with high potential for biomedical applications due to antibacterial activity against various pathogenic bacteria microbes, e.g., Escherichia coli (E. coli) and Staphylococcus aureus (S. aureus). Additionally, $BiVO_4$ has been studied as an ideal starting material for antioxidant surveillance under visible light irradiation, for detection of antioxidant capacity in the foodstuff monitoring, opening up a bright future for these materials also in the cosmetic and healthcare areas. Moreover, the $BiVO_4$ as biosensor can be applied in the fields of multi-tumor or viral biomarker detection. Due to good visible light responsiveness and stable optoelectrical

 doi:10.20944/preprints202507.0958.v1

properties, $BiVO_4$-based structures have also been studied for photoanode for efficient water splitting and hydrogen production, as well as high-performance photoelectrochemical sensors.

Looking into the future, research on the $BiVO_4$-based structures should be focused on developing novel synthesis techniques for nanostructure design and for the industrial-scale production processes, with the aim of improving the charge separation efficiency, the photocatalytic performance, the antibacterial activity and photoelectrochemical efficiency. These goals may be achieved by controlling the crystallographic orientation and long-term stability of $BiVO_4$ -based photoanodes. As to the existing concern for the preservation of the environment, continuous exploration and optimization of $BiVO_4$-based structures in the field of PEC water splitting will certainly significantly contribute to the development of a global system in the direction of clean, renewable and sustainable energy.

Author Contributions: Conceptualization, D.M. and M.F.; methodology, D.M.; software, G.C.R. and M.F.; validation, D.M. G.C.R., and M.F.; resources, D.M. and M.F.; writing—original draft preparation, D.M..; writing—review and editing, D.M. G.C.R. and M.F; funding acquisition, D.M. and M.F. All authors have read and agreed to the published version of the manuscript.

Funding: This research was supported by the Ministry of Science, Technological Development and Innovation of the Republic of Serbia (grant number 451-03-136/2025-03/ 200017).

Data Availability Statement: This review article does not contain any original data. All data ref-erenced in the article are publicly available from the sources cited in the references. No new da-tasets were generated or analyzed for this work.

Conflicts of Interest: The authors declare no conflicts of interest.

References

1. Khader, E.H.; Muslim, S. A.; Saady, N.M.C.N.; Ali, S.; Salih, I.K.; Mohammed, T.J.; Albayati, T.M.; Zendehboudi, S. Recent advances in photocatalytic advanced oxidation processes for organic compound degradation: A review. *Desalination and Water Treatment* **2024**, *318*, 100384, https://doi.org/10.1016/j.dwt.2024.100384
2. Yang, F.; Yu, X.; Wang, K.; Liu, Z.; Gao, Z.; Zhang, T.; Niu, J.; Zhao, J.; Yao, B. Photocatalytic degradation of methylene blue over $BiVO_4$/$BiPO_4$/rGO heterojunctions and their artificial neural network model. *J. Alloys Compd.* 2023, *960*, 170716, https://doi.org/10.1016/j.jallcom.2023.170716
3. Park, Y.; McDonald, K.J.; Choi, K.-S. Progress in bismuth vanadate photoanodes for use in solar water oxidation, *Chem. Soc. Rev.* 2013, *42*, 2321–2337, https://doi.org/10.1039/C2CS35260E.
4. Nguyen, T.D.; Nguyen, VH.; Nanda, S.; Vo, D.-V.N.; Nguyen, V.H.; Tran, T.V.; Nong, L.X.; Nguyen, T.T.; Bach, L.-G.; Abdullah, B.; Hong, S.-S.; Nguyen, T.V. $BiVO_4$ photocatalysis design and applications to oxygen production and degradation of organic compounds: a review. *Environ. Chem. Lett*. 2020, *18*, 1779-1801, https://doi.org/10.1007/s10311-020-01039-0.
5. Kudo, A.; Ueda, K.; Kato, H.; Mikami, I. Photocatalytic O_2 evolution under visible light irradiation on $BiVO_4$ in aqueous $AgNO_3$ solution. *Catal. Lett.* 1998, *53*, 229-230, https://doi.org/10.1023/A:1019034728816.
6. Suarez, C.M.; Hernández, S.; Russo, N. $BiVO_4$ as photocatalyst for solar fuels production through water splitting: A short review. *Appl. Catal. A Gen.* 2015, *504*, 158-170, https://doi.org/10.1016/j.apcata.2014.11.044.
7. Li, Z.; Luo, W.; Zhang, M.; Feng, J.; Zou, Z. Photoelectrochemical cells for solar hydrogen production: Current state of promissing photoelectrodes, methods to improve their properties, and outlook. *Energy Environ. Sci.* 2013, *6*, 347–370, https://doi.org/10.1039/C2EE22618A.
8. Qiao, R.; Mao, M.; Hu, E.; Zhong, Y.; Ning, J.; Hu, Y. Facile formation of mesoporous $BiVO_4$/Ag/AgCl heterostructured microspheres with enhanced visible-light photoactivity. *Inorg. Chem.* 2015, *54*, 9033–9039, https://doi.org/10.1021/acs.inorgchem.5b01303.
9. Thalluri, S.M.; Hernández, S.; Bensaid, S.; Saracco, G.; Russo, N. Green-synthesized W- and Mo-doped $BiVO_4$ oriented along the {0 4 0} facet with enhanced activity for the sun-driven water oxidation. *Appl. Catal. B Environ.* 2016, *180*, 630-636, https://doi.org/10.1016/j.apcatb.2015.07.029.

 doi:10.20944/preprints202507.0958.v1

10. Nagabhushana, G.P.; Tavakoli, A.H.; Navrotsky, A. Energetics of bismuth vanadate. *J. Solid State Chem.* 2015, *225*, 187-192, https://doi.org/10.1016/j.jssc.2014.12.030.
11. Saison, T.; Chemin, N.; Chanéac, C.; Durupthy, O.; Mariey, L.; Maugé, F.; Brezová, V.; Jolivet, J.-P. New insights into $BiVO_4$ properties as visible light photocatalyst. J. Phys. Chem. C. 2015, *119*, 12967-12977, https://doi.org/10.1021/acs.jpcc.5b01468.
12. Iwase, A.; Kato, H.; Kudo, A.; A simple preparation method of visible-light-driven $BiVO_4$ photocatalysts from oxide starting materials (Bi_2O_3 and V_2O_5) and their photocatalytic activities. *J. Sol. Energy Eng*. 2010, *132*, 021106 (5 pages).
13. Nguyen, T.D.; Nguyen, V.H.; Nanda, S.; Vo, D.-V.N.; Nguyen, V.H.; Tran, T.V.; Nong, L.X.; Nguyen, T.T.; Bach, L.-G.; Abdullah, B.; Hong, S.-S.; Nguyen, T.V. $BiVO_4$ photocatalysis design and applications to oxygen production and degradation of organic compounds: a review. *Environ. Chem. Lett*. 2020, *18*, 1779-1801, https://doi.org/10.1007/s10311-020-01039-0.
14. Zhong, X.; Li, Y.; Wu, H.; Xie, R. Recent progress in $BiVO_4$-based heterojunction nanomaterials for photocatalytic applications. *Mater. Sci. Eng. B 2023, 289, 116278,* https://doi.org/10.1016/j.mseb.2023.116278.
15. Zhao, W.; Liu, Y.; Wei, Z.; Yang, S.; He, H.; Sun, C. Fabrication of a novel p–n heterojunction photocatalyst n-$BiVO_4$@p-MoS_2 with core–shell structure and its excellent visible-light photocatalytic reduction and oxidation activities. *Appl. Catal. B-Environ.* 2016, *185*, 242-252, https://doi.org/10.1016/j.apcatb.2015.12.023.
16. Srinivasan, N.; Sakai, E.; Miyauchi, M. Balanced excitation between two semiconductors in bulk heterojunction Z-scheme system for overall water splitting. *ACS Catal.* 2016, *6*, 2197-2200, https://doi.org/10.1021/acscatal.6b00267.
17. Xie, M.; Feng, Y.; Fu, X.; Luan, P.; Jing, L. Phosphate-bridged TiO_2-$BiVO_4$ nanocomposites with exceptional visible activities for photocatalytic water splitting. *J. Alloys Compd.* 2015, *631*, 120-124, https://doi.org/10.1016/j.jallcom.2015.01.091.
18. Lv, Y.-R.; Liu, C.-J.; He, R.-K.; Li, X.; Xu, Y.-H. $BiVO_4$/TiO_2 heterojunction with enhanced photocatalytic activities and photoelectochemistry performances under visible light illumination. *Mater. Res. Bull.* 2019, *117*, 35-40, https://doi.org/10.1016/j.materresbull.2019.04.032.
19. Wang, Y.; Wang, W.; Mao, H.; Lu, Y.; Lu, J.; Huang, J.; Ye, Z.; Lu, B. Electrostatic self-assembly of $BiVO_4$-reduced graphene oxide nanocomposites for highly efficient visible light photocatalytic activities, *ACS Appl. Mater. Interfaces* 2014, *6*, 12698–12706, https://doi.org/10.1021/Am502700p.
20. Phu, N.D.; Hoang, L.H.; Guo, P.-C.; Chen, X.-B.; Chou, W.C. Study of photocatalytic activities of Bi_2WO_6/$BiVO_4$ nanocomposites. *J. Sol-Gel Sci. Technol.* 2017, *83*, 640–646, https://doi.org/10.1007/s10971-017-4450-8.
21. Cai, L.; Kisch, H. Visible light induced photoelectrochemical properties of n-$BiVO_4$ and n-$BiVO_4$/p-Co_3O_4. *Phys. Chem. C* 2008, *112*, 548–554, https://doi.org/10.1021/jp075605x.
22. Li, J.; Lu, P.; Deng, W.; Zeng, Z.; Lin, L. Zhao, G. Facile synthesis of sheet-like $BiVO_4$/$Bi_4V_2O_{11}$ composite for enhanced photocatalytic properties. *Mater. Chem. Phys.* 2020, *254*, 123489, https://doi.org/10.1016/j.matchemphys.2020.123489.
23. Qi, X.; Gu, M.; Zhu, X.; Wu, J.; Wu, Q.; Long, H.; He, K. Controlled synthesis of Ag_3PO_4/$BiVO_4$ composites with enhanced visible-light photocatalytic performance for the degradation of RhB and 2, 4-DCP. *Mater. Res. Bull.* 2016, *80*, 215-222, https://doi.org/10.1016/j.materresbull.2016.03.025.
24. Xiong, B.; Wu,Y.; Du, J.; Li, J.; Liu,B.; Ke, G.; He, H.; Zhou, Y. $Cu_3Mo_2O_9$/$BiVO_4$ heterojunction films with integrated thermodynamic and kinetic advantages for solar water oxidation. *ACS Sustainable Chem. Eng.* 2020, *8*, 14082–14090, https://doi.org/10.1021/acssuschemeng.0c04561.
25. Zhang, T.; Wang, X.; Sun, Z.; Liang, Q.; Zhou, M.; Xu, S.; Li, Z.; Sun, D. Fabrication and efficient photocatalytic dye degradation over Z-scheme-based $BiVO_4$/CdS heterojunction under visible-light irradiation. *J. Mater. Sci: Mater Electron*. 2020, *31*, 15742–15750, https://doi.org/10.1007/s10854-020-04136-6.
26. Guo, Y.; Ao, Y.; Wang, P.; Wang, C. Mediator-free direct dual-Z-scheme Bi_2S_3/$BiVO_4$/$MgIn_2S_4$ composite photocatalysts with enhanced visible-light-driven performance towards carbamazepine degradation. *Appl. Catal. B-Environ.* 2019, *254*, 479-490, https://doi.org/10.1016/j.apcatb.2019.04.031.

 doi:10.20944/preprints202507.0958.v1

27. Zhao, Z.; Bian, J.; Zhao, L.; Wu, H.; Xu, S.; Sun , L.; Li, Z.; Zhang, Z.; Jing,L. Construction of 2D Zn-MOF/$BiVO_4$ S-scheme heterojunction for efficient photocatalytic CO_2 conversion under visible light irradiation. *Chinese J. Catal.* 2022, *43*, 1331-1340, https://doi.org/10.1016/S1872-2067(21)64005-6.
28. Song, A.; Zhang, Y.; Li, Z.; Hu, J. $BiVO_4$/$CuBi_2O_4$ heterojunction photoanodes with enhanced charge separation for efficient photoelectrochemical water splitting. *Mater. Sci. Eng. B* 2024, *302*, 117241,· https://doi.org/10.1016/j.mseb.2024.117241.
29. Gao, F.; Yang, H.; Nan, C.; Zhou, W.; Gao, N.; Jia, Y.; Zhang, Y.; Chen, R. Efficient CO_2 reduction to formate using a Cu-doped $BiVO_4$ electrocathode in a WO_3 photoanode-assisted photoelectrocatalytic system. *J. Electroanal. Chem.* 2023, *930*, 117146, https://doi.org/10.1016/j.jelechem.2023.117146.
30. Ghaware, R.C.; Birajdar, N.B.; Kamble, G.S.; Kolekar, S.S. Degradation of organic Pollutant by using of $BiVO_4$–$NiFe_2O_4$ heterostructure photocatalyst under visible light irradiation: assessment of detoxicity study using *Cirrhinus mrigala*. *Langmuir* 2024, *40*, 14426–14439, https://doi.org/10.1021/acs.langmuir.4c01136.
31. Xu, H.; Wu, C.; Li, H.; Chu, J.; Sun, G.; Xu, Y.; Yan, Y. Synthesis, characterization and photocatalytic activities of rare earth-loaded $BiVO_4$ catalysts. *Appl. Surf. Sci.* 2009, *256*, 597-602, https://doi.org/10.1016/j.apsusc.2009.05.102.
32. Wang, M.; Wu, L.; Zhang, F.; Gao, L.; Geng, L.; Ge, J.; Tian, K.; Chai, H.; Niu, H.; Liu, Y.; Jin, J. Doping with rare earth el-ements and loading cocatalysts to improve the solar water splitting performance of $BiVO_4$. *Inorganics* 2023, *11*, 203; https://doi.org/10.3390/inorganics11050203.
33. Guardiano, M.G.; Gonzaga, I.M.D.; Ribeiro, L.K.; da Silva, A.C.V.; Mascaro, L. H. Gd-$BiVO_4$: An efficient photoanode for pharmaceuticals degradation in contaminated waters via solar photoelectrocatalysis. *J. Chem. Eng.* 2025, *503*, 158463, https://doi.org/10.1016/j.cej.2024.158463.
34. Liu, B.; Yan, X.; Yan, H.; Yao, Y.; Cai, Y.; Wei, J.; Chen, S.; Xu, X.; Li, L. Preparation and characterization of Mo doped in $BiVO_4$ with enhanced photocatalytic properties. *Materials* 2017, *10*, 976, https://doi.org/10.3390/ma10080976.
35. Su, W.; Lu, Z.; Shi, Q.; Cheng, C.; Liu, C.; Lu, C.; Xie, H.; Lu, B.; Huang, K.; Xu, M.; Xu, C.; Pan, H.; Zhao, C. Surface states of Mo-doped $BiVO_4$ nanoparticle-based photoanodes for photoelectrochemical degradation of chloramphenicol. *ACS Appl. Nano Mater.* 2024, *7*, 14232–14241, https://doi.org/10.1021/acsanm.4c01743.
36. Wang, G.-L.; Shan, L.-W.; Wu, Z.; Dong, L.-M. Enhanced photocatalytic properties of molybdenum-doped $BiVO_4$ prepared by sol–gel method. *Rare Met.* 2017, *36*, 129-133, https://doi.org/10.1007/s12598-015-0669-0
37. Cen, J.; Li, S.; Zheng, J.; Pan, F. Electron polarons in the subsurface layer of Mo/W-doped $BiVO_4$ surfaces. *RSC Adv.* 2019, *9*, 819-823, https://doi.org/10.1039/C8CP01316K
38. Kubendhiran, S.; Chung, R.-J.; Yougbaré, S.; Lin, L.-Y. Rational design of W-doped $BiVO_4$ photoanode coupled with FeOOH for highly efficient photoelectrochemical catalyzing water oxidation. *Int. J. Hydrogen Energy* 2022, *47*, 27012-27022, https://doi.org/10.1016/j.ijhydene.2022.06.048
39. Lalrindiki, F.; Singh, N.P.; Singh, N.M. A review of synthesis, photocatalytic, photoluminescence and antibacterial properties of bismuth vanadate-based nanomaterial. *Inorg. Chem. Commun*. 2024, *168*, 112846, https://doi.org/10.1016/j.inoche.2024.112846
40. Fan, H.; Jiang, T.; Li, H.; Wang, D.; Wang, L.; Zhai, J.; He, D.; Wang, P.; Xie, T. Effect of $BiVO_4$ crystalline phases on the photoinduced carriers behavior and photocatalytic activity. *J. Phys. Chem. C.* 2012, *116*, 2425-2430, https://doi.org/10.1021/jp206798d.
41. Cao, X.; Gu, Yan Hailin Tian, Yanfen Fang, David Johnson, Zhiyong, Chuncheng Chen, Yingping Huang. Microemulsion synthesis of ms/tz-$BiVO_4$ composites: The effect of pH on crystal structure and photocatalytic performance. *Ceram. Int.* 2020, *46*, 20788-20797, https://doi.org/10.1016/j.ceramint.2020.05.048.
42. Zhang, X.; Ai, Z.; Jia, F.; Zhang, L.; Fan, X.; Zou, Z. Selective synthesis and visible-light photocatalytic activities of $BiVO_4$ with different crystalline phases, Mater. Chem. Phys. 2007, *103*, 162-167, https://doi.org/10.1016/j.matchemphys.2007.02.008.
43. Yu, J.; Zhang, Y. Kudo, A. Synthesis and photocatalytic performances of $BiVO_4$ by ammonia co-precipitation process. *J. Solid State Chem*. 2009, *182*, 223–228, https://doi.org/10.1016/j.jssc.2008.10.021.

 doi:10.20944/preprints202507.0958.v1

44. de la Cruz, A. M.; Pérez, U.M.G. Photocatalytic properties of $BiVO_4$ prepared by the co-precipitation method: Degradation of rhodamine B and possible reaction mechanisms under visible irradiation. *Mater. Res. Bull*. 2010, *45*, 135-141, https://doi.org/10.1016/j.materresbull.2009.09.029.
45. Wan, Y.; Wang, S.; Luo, W.; Zhao, L. Impact of preparative pH on the morphology and photocatalytic activity of $BiVO_4$. *Int. J. Photoenergy*, 2012, *2012*, 392865, https://doi.org/10.1155/2012/392865.
46. Chang, Y.-K.; Wu, Y.-S.; Lu, C.-S.; Lin, P.-F.; Wu, T.-Y. Photodegradation of alachlor using $BiVO_4$ photocatalyst under visible light irradiation, *Water Air Soil Pollut.* 2015, *226*,194, https://doi.org/10.1007/s11270-015-2452-0.
47. Saison, T.; Chemin, N.; Chanéac, C.; Durupthy, O.; Mariey, L.; Maugé, F.; Brezová, V.; Jolivet, J.-P. New insights into $BiVO_4$ properties as visible light photocatalyst *J. Phys. Chem. C* 2015, *119*, 12967-12977, https://doi.org/10.1021/acs.jpcc.5b01468.
48. Hazarika, M.; Lutukurthi, D.N.V.V.K.; Ra, V.K. Photocatalytic activity of Ho^{3+}-Yb^{3+} activated $BiVO_4$ upconverting phosphors. *J. Alloys Compd.* 2024, *1002*, 175453, https://doi.org/10.1016/j.jallcom.2024.175453.
49. Ahmed, T.; Zhang, H.-l.; Gao, Y.-Y.; Xu, H.-b.; Zhang, Yi. Surfactant-free synthesis of m-$BiVO_4$ nanoribbons and enhanced visible-light photocatalytic properties. *Mater. Res. Bull.* 2018, *99*, 298-305, https://doi.org/10.1016/j.materresbull.2017.11.029.
50. Deng, Y.; Huang, R.; Li, X.; Wang, Y.; Tian, J.; Zhu, M.; Gong, X. Surfactants modulating of $BiVO_4$ on photocatalytic property as a regulation of surface free energy. *Langmuir* 2024, *40*, 50, 26540–26550, https://doi.org/10.1021/acs.langmuir.4c03413.
51. Helal, A.; El-Sheikh, S.M.; Yu, J.; Eid, A.I.; El-Haka, S.A.; Samra, S.E. Novel synthesis of $BiVO_4$ using homogeneous precipitation and its enhanced photocatalytic activity. *J. Nanopart. Res.* 2020, *22*, 132, https://doi.org/10.1007/s11051-020-04861-3.
52. Montañés, L.; Mesa, C.A.; Gutiérrez-Blanco, A.; Robles, C.; Julián-López, B.; Giménez, S. Facile surfactant-assisted synthesis of $BiVO_4$ nanoparticulate films for solar water splitting. *Catalysts* 2021, *11*, 1244, https://doi.org/10.3390/catal11101244.
53. Zhansheng, W.; Xue, Y.; He, X.; Li, Y.; Yang, X.; Wu, Z.; Cravotto, G. Surfactants-assisted preparation of $BiVO_4$ with novel morphologies via microwave method and CdS decoration for enhanced photocatalytic properties. *J. Hazard. Mater.* 2020, *387*, 122019, https://doi.org/10.1016/j.jhazmat.2020.122019
54. Liu, J.; Li, B.; Kong, L.; Xiao, Q.; Huang, S. Surfactants-assisted morphological regulation of $BiVO_4$ nanostructures for photocatalytic degradation of organic pollutants in wastewater. *J. Phys. Chem. Solids 2023, 172,* 111079, https://doi.org/10.1016/j.jpcs.2022.111079
55. Cheng, C.; Tan, H.; Zhu, W.; Liu, L.; Chen, K.; Yan, J. The transition of tetragonal to monoclinic phase in $BiVO_4$ coupled with peroxymonosulfate for photocatalytic degradation of tetracycline hydrochloride. *Environ. Res*. 2025, *267*, 120631, https://doi.org/10.1016/j.envres.2024.120631
56. Polo, A.; Dozzi, M.V.; Marra, G.; Sivula, K.; Selli, E. Improving the photoelectrocatalytic efficiency of $CuWO_4$ through molybdenum for tungsten substitution and coupling with $BiVO_4$. *Sustain. Energy Fuels* 2024, *8*, 3182-3191, https://doi.org/10.1039/d4se00161c
57. Zhang, X.; Chen, F.-y.; Tang, Y.-b.; Liu, Y.-m.; Wang, X.-g. A rapid microwave synthesis of nanoscale $BiVO_4$/Bi_2O_3@SiO_2 with large specific surface area and excellent visible-light-driven activity. *Desalin Water Treat.* 2019, *152*, 99-107, https://doi.org/10.5004/dwt.2019.23947.
58. Chen, F.-y.; Zhang, X.; Tang, Y.-b.; Wang, X.-g.; Shu. K.-k. Facile and rapid synthesis of a novel spindle-like heterojunction $BiVO_4$ showing enhanced visible-light-driven photoactivity. *RSC Adv.* 2020, *10*, 5234-5240, https://doi.org/10.1039/C9RA07891F
59. Sanchez-Martınez, D.; Hernandez-Uresti, D.B.; Torres-Martinez, L.; Mejia-Rosales, M.S. Photocatalytic properties of $BiVO_4$ synthesized by microwave-assisted hydrothermal method under simulated sunlight irradiation. *Res. Chem. Intermed-* 2015, *41* 8839–8854, https://doi.org/10.1007/s11164-015-1932-6.
60. Tan, G.; Zhang, L.; Ren, H.; Wei, S.; Huang, J.; Xia, A. Effects of pH on the hierarchical structures and photocatalytic performance of $BiVO_4$ powders prepared via the microwave hydrothermal method. *ACS Appl. Mater. Interfaces* 2013, *5*, 5186–5193, https://doi.org/10.1021/am401019m

 doi:10.20944/preprints202507.0958.v1

61. Zhang, L.; Tan, G.; Wei, S.; Ren, H.; Xia, A.; Luo, Y. Microwave hydrothermal synthesis and photocatalytic properties of $TiO_2/BiVO_4$ composite photocatalysts. *Ceram. Int.* 2013, *39*, 8597-8604, https://doi.org/10.1016/j.ceramint.2013.03.106
62. Chen, S.-H.; Jiang, Y.-S.; Lin, H.-y. Easy synthesis of $BiVO_4$ for photocatalytic overall water splitting. *ACS Omega* 2020, *5*, 8927–8933, https://doi.org/10.1021/acsomega.0c00699.
63. Kshetri, Y.K.; Regmi, C.; Dhakal, D.R.; Kim, T.-H.; Kim, S. H. Kim, H.-S.; Lee, S. W. Microwave hydrothermal synthesis and upconversion properties of $BiVO_4$ nanoparticles. *Nanotechnology* 2020, *31*, 244001, https://doi.org/10.1088/1361-6528/ab78ae
64. Zhao, G.; Ding, J.; Zhou, F.; Zhao, Q.; Wang, K.; Chen, X.; Gao, Q. Insight into a novel microwave-assisted W doped $BiVO_4$ self-assembled sphere with rich oxygen vacancies oriented on rGO (W-$BiVO_{4-x}$/rGO) photocatalyst for efficient contaminants removal. *Sep. Purif. Technol.* 2021, *277*, 119610, https://doi.org/10.1016/j.seppur.2021.119610
65. Wang, X.; Liu, H.; Wang, J.; Chang, L.; Song, N.; Yan, Z.; Wan, X. Additive-free solvothermal preparation, characterization, and photocatalytic activity of 3D butterfly-like $BiVO_4$. *Res. Chem. Intermed*. 2015, *41*, 2465–2477, https://doi.org/10.1016/j.seppur.2021.119610.
66. Kamble, G.S.; Ling, Y.C. Solvothermal synthesis of facet-dependent $BiVO_4$ photocatalyst with enhanced visible-light-driven photocatalytic degradation of organic pollutant: assessment of toxicity by zebrafish embryo. *Sci. Rep.* 2020, *10*, 12993, https://doi.org/10.1038/s41598-020-69706-4.
67. Pham, M.Q.; Ngo, T.M.; Nguyen, V.H.; Nong, L.X.; Vo, D.-V.N.; Tran, T.V.; Nguyen, T.-D.; Bui, X.-T.; Nguyen, T.D. Facile solvothermal synthesis of highly active monoclinic scheelite $BiVO_4$ for photocatalytic degradation of methylene blue under white LED light irradiation. *Arab. J. Chem*. 2020, *13*, 8388-8394, https://doi.org/10.1016/j.arabjc.2020. 05.029.
68. Wang, S.; Zhao, L.; Huang, W.; Zhao, H.; Chen, J.; Cai, Q.; Jiang, X.; Lu, C.; Shi, W. Solvothermal synthesis of CoO/$BiVO_4$ p-n heterojunction with micro-nano spherical structure for enhanced visible light photocatalytic activity towards degradation of tetracycline. *Mater. Res. Bull*. 2021, *135*, 111161, https://doi.org/10.1016/j.materresbull.2020.111161.
69. Wang, M.; Guo, Y.; Wang, Z.; Cui, H.; Sun, T.; Tang, Y. Simple glycerol-assisted and morphology controllable solvothermal synthesis of $CeVO_4/BiVO_4$ hierarchical hollow microspheres with enhanced photocatalytic activities. *Mater. Chem. Front.* 2021, *5*, 6522-6529, https://doi.org/10.1039/D1QM00770J.
70. Li, B.; Wang, W.; Shi, J.; Zhang, Y.; Liu, X.; Dong, P.; Xi X. Development of Z-scheme $Bi_5O_7I/BiVO_4$ heterostructure for efficient photocatalytic water splitting activity. *Colloids Surf. A: Physicochem. Eng. Asp.* 2025, *713*, 136472, https://doi.org/10.1016/j.colsurfa.2025.136472.
71. Yu, S.; Su, C.; Xiao, Z.; Kuang, Y.; Gong, X.; He, X.; Liu, J.; Jin, Q.; Sun, Z. Tuning surface hydrophilicity of a $BiVO_4$ photoanode through interface engineering for efficient PEC water splitting. *RSC Adv.*2025, *15*, 815-823, https://doi.org/10.1039/d4ra08254k.
72. Yu, J.; Zhang, Y.; Kudo, A. Synthesis and photocatalytic performances of $BiVO_4$ by ammonia co-precipitation process. *J. Solid State Chem.* 2009, *182*, 223-228, https://doi.org/10.1016/j.jssc.2008.10.021.
73. Nguyen, T.D.; Cao, V.D.; Nguyen, V.H.; Nong, L.X.; Luu, T. D.; Vo, D.-V.N.; Do, S.T.; Lam, T.D. Synthesized $BiVO_4$ was by the co-precipitation method for Rhodamine B degradation under visible light. *IOP Conf. Ser.: Mater. Sci. Eng*. 2019, *542*, 012058, https://doi.org/10.1088/1757-899X/542/1/012058.
74. Vinothkumar, V.; Sangili, A.; Chen, S.-M.; Abinaya, M. Additive-free synthesis of $BiVO_4$ microspheres as an electrochemical sensor for determination of antituberculosis drug rifampicin. *Colloids Surf. A: Physicochem. Eng. Asp.* 2021, *624*, 126849, https://doi.org/10.1016/j.colsurfa.2021.126849.
75. Riapanitra, A.; Setyaningtyas, T.; Haryanto, M.J.; Haryadinaru, G.H. Hydrothermal and coprecipitation synthesis design of $BiVO_4$ for Methylene blue degradation . *J. Ris. Kim*. 2025, *16*, 20-32, https://doi.org/10.25077/jrk.v16i1.740.
76. Xie, Y.; Wu, H.; Luo, J.; Zhang, S.; Wang, L.; Wang, X.; Ma, Y.; Ning, P. Phase transition guided V_2O_5/β-Bi_2O_3 Z-scheme heterojunctions for efficient photocatalytic Hg^0 oxidation. *Sep. Purif. Technol.* 2024, *330*, 125318, https://doi.org/10.1016/j.seppur.2023.125318.

 doi:10.20944/preprints202507.0958.v1

77. Phu, N.D.; Hoang, L.H.; Vu, P.K.; Kong, M.-H.; Chen, X.-B.; Wen, H. C. W. Chou, C. Control of crystal phase of $BiVO_4$ nanoparticles synthesized by microwave assisted method. *J. Mater. Sci. Mater. Electron.* 2016, *27*, 6452-6456, https://doi.org/10.1007/s10854-016-4585-3.
78. Sun, Q.; Qiao, F.; Zhou, T. CTAB assisted hydrothermal synthesis of oxygen vacancy enriched $BiVO_4$ for enhanced photocatalytic hydrogen production. *CrystEngComm* 2025, *27*, 948-955, https://doi.org/10.1039/D4CE01284D.
79. Yan, M.; Yan, Y.; Wu, Y.; Shi, W.; Hua, Y. Microwave-assisted synthesis of monoclinic–tetragonal $BiVO_4$ heterojunctions with enhanced visible-light-driven photocatalytic degradation of tetracycline, *RSC Adv.* 2015, *5*, 90255-90264, https://doi.org/10.1039/C5RA13684A.
80. Chen, S.-H.; Jiang, Y.-S.; Lin, H.-y. Easy synthesis of $BiVO_4$ for photocatalytic overall water splitting. *ACS Omega* 2020, 5, 8927–8933, https://doi.org/10.1021/acsomega.0c00699
81. Shafi, I.; Liang, E.; Li, B.; Self-assembled $BiVO_4$ nanorods: A fascinating electrode material for highly efficient pseudocapacitors and electrochemical nitrite sensors. *J. Phys. Chem. Solids* 2022, *162*, 110517, https://doi.org/10.1016/j.jpcs.2021.110517.
82. Heckel, S.; Wittmann, M.; Reid, M.; Villa, K.; Simmchen, J. An account on $BiVO_4$ as photocatalytic active matter. *Acc. Mater. Res.* 2024, *5*, 400–412, https://doi.org/10.1021/accountsmr.3c00021.
83. Kudo, A.; Omori, K.; Kato, H. A novel aqueous process for preparation of crystal form-controlled and highly crystalline $BiVO_4$ powder from layered vanadates at room temperature and its photocatalytic and photophysical properties. *J. Am. Chem. Soc.* 1999, *121*, 11459–11467, https://doi.org/10.1021/ja992541y.
84. Ribeiro, F.W.P.; Gromboni, M.F.; Marken, F.; Mascaro, L.H. Photoelectrocatalytic properties of $BiVO_4$ prepared with different alcohol solvents. *Int. J. Hydrogen Energy* 2016, *41*, 17380-17389, https://doi.org/10.1016/j.ijhydene.2016.07.159.
85. Liu, Y.; Ma, J.; Liu, Z.; Dai, C.; Song, Z.; Sun, Y.; Fang, J.; Zhao, J. Low-temperature synthesis of $BiVO_4$ crystallites in molten salt medium and their UV–vis absorption. *Ceram. Int.* 2010, *36*, 2073-2077, https://doi.org/10.1016/j.ceramint.2010.06.003.
86. Cheng, B.; Lou, H., Zeng, Z.; Liu, Y.; Zeng, Q. Structural phase transition in $BiVO_4$ nanosheets under high pressure. *J. Phys. Chem. C* 2024, *128*, 12267–12273, https://doi.org/10.1021/acs.jpcc.4c03113]
87. Zhao, Z.; Ling, Q.; Deng, S.; Li, Z.; Lv, J.; Yang, L.; Cao, C.; Sun, Z.; Zhang, M. Photocatalytic degradation of tetracycline hydrochloride using a $BiVO_4$/MIL-88B(Fe) heterojunction, *New J. Chem.* 2024, *48*, 9442-9456, https://doi.org/10.1016/j.envres.2024.120631
88. Miersch, L.; Rüffer, T.; Schlesinger, M.; Lang, H.; Mehring, M. Hydrolysis studies on bismuth nitrate: synthesis and crystallization of four novel polynuclear basic bismuth nitrates. *Inorg. Chem.* 2012, *51*, 9376–9384, https://doi.org/10.1021/ic301148p.
89. Pang, J.; Han, Q.; Liu, W.; Shen, Z.; Wang, X.; Zhu, J. Two basic bismuth nitrates: $[Bi_6O_6(OH)_2](NO_3)_4$ $2H_2O$ with superior photodegradation activity for rhodamine B and $[Bi_6O_5(OH)_3](NO_3)_5{\cdot}3H_2O$ with ultrahigh adsorption capacity for methyl orange. *App. Surf. Sci.* 2017, 422, 283–294, https://doi.org/10.1016/j.apsusc.2017.06.022.
90. Dolić, S.D.; Jovanović, D.J.; Smits, K.; Babić, B.; Marinović-Cincović, M.; Porobić, S.; Dramićanin, M.D. A comparative study of photocatalytically active nanocrystalline tetragonal zyrcon-type and monoclinic scheelite-type bismuth vanadate. *Ceram. Int.* 2018, 44, 17953-17961, https://doi.org/10.1016/j.ceramint.2018.06.272.
91. Dolić, S.D.; Jovanović, D.J.; Štrbac, D.; Đačanin Far, Lj.; Dramićanin, M.D. Improved coloristic properties and high NIR reflectance of environment-friendly yellow pigments based on bismuth vanadate, *Ceram. Int.* 2018, *44*, 22731-22737, https://doi.org/10.1016/j.ceramint.2018.09.057.
92. Marinković, D.; Righini, G.C.; Ferrari, M. Synthesis, optical, and photocatalytic properties of the $BiVO_4$ semiconductor nanoparticles with tetragonal zircon-type structure, *Photonics* 2025, *12*, 438; https://doi.org/10.3390/photonics12050438.
93. Nguyena, T.D.; Hong, S.-Soo. Facile solvothermal synthesis of monoclinic-tetragonal heterostructured $BiVO_4$ for photodegradation of rhodamine B. *Catal. Commun.* 2020, *136*, 105920, https://doi.org/10.1016/j.catcom.2019.105920.

 doi:10.20944/preprints202507.0958.v1

94. Esmaili, Z.; Sadeghian, Z.; Ashrafizadeh, S.N. Tailoring of $BiVO_4$ morphology for efficient antifouling of visible-light-driven photocatalytic ceramic membranes for oily wastewater treatment. *J. Water Process Eng.* 2024, *67*, 106145, https://doi.org/10.1016/j.jwpe.2024.106145
95. Li, J.-Q.; Guo, Z.-Y; Wang, D.-F.; Lui, H.; Du, J.; Zhu, Z.-F. Effects of pH value on the surface morphology of $BiVO_4$ microspheres and removal of methylene blue under visible light. J. Exp. Nanosci. 2014, 9, 616–624, https://doi.org/10.1080/17458080.2012.680931.
96. Huang, J.G.; Wang, B.; Pang, S.; Zhang, X.Y.; Yang, X. Y., Guo, X.T.; Wang, X.S. Effects of pH value and hydrothermal time on the structure and photocatalytic activity of monoclinic-scheelite $BiVO_4$. Optoelectron. Adv. Mater. Rapid Commun. 2015, 9, 1273–1279.
97. Dong, S.; Xia, L.; Zhang, F.; Li, F.; Wang, Y.; Cu,i L.; Feng, J.; Sun, J. Effects of pH value and hydrothermal treatment on the microstructure and natural-sunlight photocatalytic performance of $ZnSn(OH)_6$ photocatalyst. J. Alloys Compd. 2019, 810, 151955, https://doi.org/10.1016/j.jallcom.2019.151955.
98. Sun, M.; Guo, P.; Wang, M.; Ren, F. The effect of pH on the photocatalytic performance of $BiVO_4$ for phenol mine sewage degradation under visible light. Optik 2019, 179, 672–679, https://doi.org/10.1016/j.ijleo.2018.10.211.
99. Kim, M.-W.; Samuel, E.; Kim, K.; Yoon, H.; Joshi, B.; Swihart, M.T.; Yoon, S.S. Tuning the morphology of electrosprayed $BiVO_4$ from nanopillars to nanoferns via pH control for solar water splitting. J. Alloys Compd. 2018, 769, 193-200, https://doi.org/10.1016/j.jallcom.2018.07.167.
100. Wang, L.; Su, J.; Guo, L. Self-assembly synthesis of monodisperse $BiVO_4$ nanosphere via a hybrid strategy for photoelectrochemical water splitting. *ChemCatChem* 2020, *12*, 5269-5275, https://doi.org/10.1002/cctc.202000975.
101. Li, F.; Yang, C.; Li, Q.; Cao, W.; Li, T. The pH-controlled morphology transition of $BiVO_4$ photocatalysts from microparticles to hollow microspheres. *Mater. Lett.* 2015, *145*, 52-55, https://doi.org/10.1016/j.matlet.2015.01.043.
102. Sun, W.; Xie, M.; Jing, L.; Luan, Y.; Fu, H. Synthesis of large surface area nano-sized $BiVO_4$ by an EDTA-modified hydrothermal process and its enhanced visible photocatalytic activity. *J. Solid State Chem*. 2011, *184*, 3050–3054, https://doi.org/10.1016/j.jssc.2011.09.013.
103. Mao, J.; Wu, Q.; Tao, F.; Xu, W.; Hong, T.; Dong Y. Facile fabrication of porous $BiVO_4$ hollow spheres with improved visible-light photocatalytic properties. *RSC Adv.* 2020, *10*, 6395-6404, https://doi.org/10.1039/D0RA00698J.
104. Yin, W.; Wang, W.; Shang, M.; Zhou, L.; Sun, S.; Wang, L. $BiVO_4$ hollow nanospheres: anchoring synthesis, growth mechanism, and their application in photocatalysis. *EurJIC* 2009, *2009*, 4379-4384, https://doi.org/10.1002/ejic.200900614.
105. Dong, L.; Guo, S.; Zhu, S.; Xu, D.; Zhang, L.; Huo, M.; Yang, X. Sunlight responsive $BiVO_4$photocatalyst: Effects of pH on L-cysteine-assisted hydrothermal treatment and enhanced degradation of ofloxacin. *Catal. Commun*. 2011, *16*, 250–254, https://doi.org/10.1016/j.catcom.2011.05.005.
106. Xia, G.; Ye, J. Synthesis of bismuth vanadate nanoplates with exposed {001} facets and enhanced visible-light photocatalytic properties. *Chem. Commun*. 2010, *46*, 1893–1895, https://doi.org/10.1039/B923435G
107. Ma, Y.; Jiang, H.; Zhang, X.; Xing, J. Yunsheng Guan, Synthesis of hierarchical m-$BiVO_4$ particles via hydro-solvothermal method and their photocatalytic properties. *Cer. Inter*. 2014, *4*, 16485–16493, https://doi.org/10.1016/j.ceramint.2014.07.158.
108. Wang, X.; Liu, H.; Wang, J.; Chang, L.; Song, N.; Yan, Z.; Wan, X. Additive-free solvothermal preparation, characterization, and photocatalytic activity of 3D butterfly-like $BiVO_4$. *Res. Chem. Intermed*. 2015, 412, 465–2477, https://doi.org/10.1007/s11164-013-1360-4.
109. Chen, L.; Wang, J.; Meng, D.; Xing, Y.; Tian, X.; Yu, X.; Xu, K.; Wu, X. Effects of citric acid and urea on the structural and morphological characteristics of $BiVO_4$ synthesized by the sol–gel combustion method, *J. Sol-Gel Sci. Technol.* 2015, *76*, 562–571, https://doi.org/10.1007/s10971-015-3806-1.
110. Adán, C.; Marugán, J.; Obregón, S.; Colón, G. Photocatalytic activity of bismuth vanadates under UV-A and visible light irradiation: Inactivation of Escherichia coli vs oxidation of methanol. *Catal. Today* 2015, *240*, 93–99, https://doi.org/10.1016/j.cattod.2014.03.059.

 doi:10.20944/preprints202507.0958.v1

111. Sanchez-Martınez, D.; Hernandez-Uresti, D.B.; Torres-Martinez, L.M.; Mejia-Rosales, S. Photocatalytic properties of $BiVO_4$ synthesized by microwave-assisted hydrothermal method under simulated sunlight irradiation, *Res. Chem. Intermed*. 2015, *41*, 8839–8854, https://doi.org/10.1007/s11164-015-1932-6.
112. Y.-K.; Chang, Wu, Y.-S.; Chung-Lu, S.; Lin, P.-F.; Wu, T.-Y.; Photodegradation of alachlor using $BiVO_4$ photocatalyst under visible light irradiation. *Water Air Soil Pollut.* 2015, *226*, 194, https://doi.org/10.1007/s11270-015-2452-0.
113. Liu, X.; Chen, W.; Wang, W.; Jiang, Y.; Cao, K.; Jiao, Z. F- regulate the preparation of polyhedral $BiVO_4$ enclosed by High-Index facet and enhance its photocatalytic activity. *J. Colloid Interface Sci.* 2022, *606*, 393-405, https://doi.org/10.1016/j.jcis.2021.08.023.
114. Ravidhas, C.; Josephine, A.J.; Sudhagar, P.; Devadoss, A.; Terashima, C.; Nakata, K.; Fujishima, A.; Raj, A.M.E.; Sanjeeviraja, C.; Pitchaimuthu, S. Facile synthesis of nanostructured monoclinic bismuth vanadate by a co-precipitation method: Structural, optical and photocatalytic properties. *Mat. Sci. Semicon. Proc.* 2015, *30*, 343–351, https://doi.org/10.1016/j.mssp.2014.10.026.
115. Zhang, Y.; Li, G.; Yang, X.; Yang, H.; Lu, Z.; Chen, R. Monoclinic $BiVO_4$ micro-/nanostructures: Microwave and ultrasonic wave combined synthesis and their visible-light photocatalytic activities. *J. Alloys Compd*. 2013, *551*, 544–550, https://doi.org/10.1016/j.jallcom.2012.11.017.
116. Lin, X.; Yu, L.; Yan, L.; Li, H.; Yan, Y.; Liu, C.; Zhai, H. Visible light photocatalytic activity of $BiVO_4$ particles with different morphologies. *Solid State Sci.* 2014, *32*, 61-66, https://doi.org/10.1016/j.solidstatesciences.2014.03.018.
117. Zhang, H.M.; Liu, J.B.; Wang, H.; Zhang, W.X.; Yan, H. Rapid microwave-assisted synthesis of phase controlled $BiVO_4$ nanocrystals and research on photocatalytic properties under visible light irradiation. *J. Nanopart. Res.* 2008, *10*, 767-774, https://doi.org/10.1007/s11051-007-9310-y.
118. Trinh, D.T.T.; Khanitchaidecha, W.; Channei, D.; Nakaruk, A. Synthesis, characterization and environmental applications of bismuth vanadate. *Res. Chem. Intermed*. 2019, *45*, 5217–5259 https://doi.org/10.1007/s11164-019-03912-2
119. Zhong, X.; Li, Y.; Wu, H.; Xie, R. Recent progress in $BiVO_4$-based heterojunction nanomaterials for photocatalytic applications. *Mater. Sci. Eng. B* 2023, *289*, 116278, https://doi.org/10.1016/j.mseb.2023.116278
120. Wu, S M.; Jing, Q.; Feng, X.; Chen, L. $BiVO_4$ microstructures with various morphologies: Synthesis and characterization. Appl. Surf. Sci. 2018, 427, 525-532, https://doi.org/10.1016/j.apsusc.2017.07.299.
121. Qurashi, M.M.; Barnes, W.H.A Preliminary structure for pucherite, $BiVO_4$. *Am. Mineral*. 1952, *37*,423–426. 68.
122. Zhou, D.; Pang, L.X.; Wang, D.W.; Reaney, I M. $BiVO_4$ based high K microwave dielectric materials: A Review. *J. Mater. Chem. C* 2018, *6*, 9290–9313, https://doi.org/10.1039/C8TC02260G.
123. Jovanović, D.J.; Chiappini, A.; Zur, L.; Gavrilović, T.V.; Tran, T.N.L.; Chiasera, A.; Lukowiak, A.; Smits, K.; Dramićanin, M.D.; Ferrari, M. Synthesis, structure and spectroscopic properties of luminescent $GdVO_4:Dy^{3+}$ and $DyVO_4$ particles, *Opt. Mater.* 2018,
124. *76*, 308-316, https://doi.org/10.1016/j.optmat.2017.12.046.
125. Sleight, A. W.; Chen, H.-y.; Ferretti, A.; Cox, D. E. Crystal growth and structure of $BiVO_4$, *Mater. Res. Bull.* 1979, 14, 1571–1581, https://doi.org/10.1016/0025-5408(72)90227-9.
126. Tokunaga, S.; Kato, H.; Kudo, A. Selective preparation of monoclinic and tetragonal $BiVO_4$ with scheelite structure and their photocatalytic properties. *Chem. Mater*. 2001, *13*, 4624–4628, https://doi.org/10.1021/cm0103390.
127. Park, Y.; McDonald, K. J.; Choi, K. S. Progress in bismuth vanadate photoanodes for use in solar water oxidation. *Chem. Soc. Rev.* 2013, *42*, 2321–2337, https://doi.org/10.1039/C2CS35260E.
128. Gea, J.; Wu, L.; Gab, L.; Niu, H.; Liu,M.; Zou, Y.; Wang, J.; Jin, J. Green light all the way: Triple modification synergistic modification effect to enhance the photoelectrochemical water oxidation performance of $BiVO_4$ photoanode, *J. Colloid Interface Sci.* 2025, *677*, 90–98, https://doi.org/10.1016/j.jcis.2024.07.203.
129. Park, H. S.; Kweon, K. E.; Ye, H.; Paek, E.; Hwang, G. S.; Bard, A. J. Factors in the metal doping of $BiVO_4$ for improved photoelectrocatalytic activity as studied by scanning electrochemical microscopy and first-principles density-functional calculation. *J. Phys. Chem. C* 2011, *115*, 1787017879, https://doi.org/10.1021/jp204492r.

 doi:10.20944/preprints202507.0958.v1

130. Abdellaoui, I.; Islam, M.M.; Remeika, M.; Higuchi, Y.; Kawaguchi, T.; Harada, T.; Budich, C.; Maeda, T.; Wada, T.; Ikeda, S.; Sakurai, T. Photocarrier recombination dynamics in $BiVO_4$ for visible light-driven water oxidation, *J. Phys. Chem. C* 2020, *124*, 39623972, https://doi.org/10.1021/acs.jpcc.9b10621.
131. Ravensbergen, J.; Abdi, F.F.; van Santen, J. H.; Frese, R.N.; Dam, B.; van de Krol, R.; Kennis, J.T.M. Unraveling the Carrier Dynamics of $BiVO_4$: A femtosecond to microsecond transient absorption study, *J. Phys. Chem. C* 2014, *118*, 2779327800.
132. Suzuki, Y.; Murthy, D. H.K.; Matsuzaki, H.; Furube, A.; Wang, Q.; Hisatomi, T.; Domen, K.; Seki, K. Rational interpretation of correlated kinetics of mobile and trapped charge carriers: analysis of ultrafast carrier dynamics in $BiVO_4$, *J. Phys. Chem. C* 2017, *121*, 1904419052, https://doi.org/10.1021/acs.jpcc.7b05574.
133. Ma, Y.; Pendlebury, S.R.; Reynal, A.; Formal, L.F.; Durrant, J.R. Dynamics of photo generated holes in undoped $BiVO_4$ photoanodes for solar water oxidation. *Chem. Sci.* 2014, *5*, 29642973, https://doi.org/10.1039/C4SC00469H.
134. Merupo, V.; Velumani, S.; Oza, G.; Makowska-Janusik, M.; Kassiba, A. Structural, electronic and optical features of molybdenum-doped bismuth vanadium oxide. *Mater. Sci. Semicond. Process*. 2015, *31*, 618623, https://doi.org/10.1016/j.mssp.2014.12.057.
135. Kalanur, S.S.; Seo, H. An experimental and density functional theory studies of Nb-doped $BiVO_4$ photoanodes for enhanced solar water splitting, J. Catal. 2022, 410, 144-155, https://doi.org/10.1016/j.jcat.2022.04.019.
136. Kunioku, H.; Higashi, M.; Tomita, O.; *Yabuuchi, M.; Kato, D.;* Fujito, H.; Kageyama, H.; Abe, R. Strong hybridization between Bi-6s and O-2p orbitals in Sillén–Aurivillius perovskite Bi_4MO_8X (M = Nb, Ta; X = Cl, Br), visible light photocatalysts enabling stable water oxidation, J. Mater. Chem. A 2018, 6, 3100-3107, https://doi.org/10.1039/C7TA08619A.
137. Tolod, K.R.; Hernández, S.; Russo, N. Recent advances in the $BiVO_4$ photocatalyst for sun-driven water oxidation: top-performing photoanodes and scale-up challenges, Catalysts 2017, 7, 13, https://doi.org/10.3390/catal7010013.
138. Nguyen, T.D.; Nguyen, VH.; Nanda, S.; Vo, D.-V.N.; Nguyen, V.H.; Tran, T.V.; Nong, L.X.; Nguyen, T.T.; Bach, L.-G.; Abdullah, B.; Hong, S.-S.; Nguyen, T.V. $BiVO_4$ photocatalysis design and applications to oxygen production and degradation of organic compounds: a review. *Environ. Chem. Lett*. 2020, *18*, 1779-1801, https://doi.org/10.1007/s10311-020-01039-0
139. Pramila, S.; Mallikarjunaswamy, C.; Ranganatha, V.L.; Nagaraju, G.; $BiVO_4$ nanoballs: a simple precipitation pathway, promising electrochemical sensor, and photodegradation under visible light, *Ionics* 2024, *30*, 2819–2838, https://doi.org/10.1007/s11581-024-05460-1.
140. Aghakhaninejad, S.; Rahimi, R.; Zargari, S. Application of $BiVO_4$ nanocomposite for photodegradation of methyl orange, ***Proceedings*** 2019, ***9***, 52; https://doi.org/10.3390/ecsoc-22-05666.
141. Sobahi, T.R. Application of $BiVO_4$-MWCNT nanocomposites for boosted photocatalytic oxidation of atrazine under visible light, *Appl. Nanosci*. 2021, *11*, 2811–2822, https://doi.org/10.1007/s13204-021-02177-9.
142. Chopade, A.S.; Kolhe, N.D.; Walekar, L.S.; Kadam, A.N.; Patil, V.A.; Al-Enizi, A.M.; Tamboli, M.S.; Mhamane, D.S.; Mali, M.G. Chemical bath assisted construction of CuO/$BiVO_4$ p-n heterojunction photocatalyst for visible light driven rapid removal of MB and Cr(VI), *Colloids Surf. A: Physicochem. Eng. Asp.* 2024, *700*, 134665, https://doi.org/10.1016/j.colsurfa.2024.134665.
143. Liapun, V.; Hanif, M.B.; Sihor, M.; Vislocka, X.; Pandiaraj, S.; Unnikrishnan, V.K.; Thirunavukkarasu, G.K.; Edelmannová, M.F.; Reli, M.; Monfort, O.; Kočí, K.; Motola, M. Versatile application of $BiVO_4/TiO_2$ S-scheme photocatalyst: Photocatalytic CO_2 and Cr(VI) reduction, *Chemosphere* 2023, *337*, 139397, https://doi.org/10.1016/j.chemosphere.2023.139397.
144. Jing, Q.; Feng, X.; Zhao, X.; Duan, Z.; Pan, J.; Chen, L.; Liu, Y. Bi/$BiVO_4$ chainlike hollow microstructures: Synthesis, characterization, and application as visible-light-active photocatalysts, *ACS Appl. Nano Mater* 2018, *1*, 2653–266, https://doi.org/10.1021/acsanm.8b00330.
145. Shi, H.; Li, C.; Zheng, R.; Wang, L.; Wang, W.; Bian, J.; Meng, X. Synergistic effect of oxygen vacancies and built-in electric field in $GdCrO_3/BiVO_4$ composites for boosted photocatalytic reduction of nitrate in water, *J. Clean. Prod.* 2023, *407*, 137088, https://doi.org/10.1016/j.jclepro.2023.137088.

 doi:10.20944/preprints202507.0958.v1

146. Jeon, H.C.; Kumar, G.M.; Lee, D.J.; Sekar, S.; Kim, D.Y.; Ilanchezhiyan, P. Fabrication of 2D/2D $InVO_4/BiVO_4$ heterojunction with synergistic effects for enhanced photocatalytic degradation and photoelectrochemical applications, *Int. J. Energy Research* 2024, *1*, 1-12, https://doi.org/10.1155/2024/8897089
147. Orimolade, B.O.; Arotiba, O.A. Towards visible light driven photoelectrocatalysis for water treatment: Application of a FTO/$BiVO_4$/Ag_2S heterojunction anode for the removal of emerging pharmaceutical pollutants, *Sci Rep* 2020, *10*, 5348, https://doi.org/10.1038/s41598-020-62425-w.
148. Alhaddad, M.; Amin, M.S. Removal of ciprofloxacin applying Pt@$BiVO_4$-g-C_3N_4 nanocomposite under visible light, *Opt. Mater.* 2022, *124*, 111976, https://doi.org/10.1016/j.optmat.2022.111976
149. Kumar, M.; Gaur, A.; Chauhan, V.S.; Vaish, R.; Kebaili, I. Tribocatalytic dye degradation using $BiVO_4$, *Ceram. Int.* 2024, *50*, 8360-8369, https://doi.org/10.1016/j.ceramint.2023.12.171.
150. Zhu, M.; Yang, S.; Wang, D.; Hogan, J. Sadrzadeh, M. CTAC-assisted monoclinic $BiVO_4$ with oxygen defects for efficient photocatalytic performances: A combined experimental and DFT study, *J. Alloys Compd.* 2024, *990*, 30, 174404, https://doi.org/10.1016/j.jallcom.2024.174404.
151. Ge, Y.-D.; Xing, M.-Y, Zhang, H.-S.; Zhou, X.-Y.; Zhang, L.; Wang, X.; Xu, L. Study on the development of an innovative type-II sonocatalyst of $BiVO_4$/$FeVO_4$ and its application in sonocatalytic removal of tetracycline, *J. Alloys Compd*. 2025, *1018*, 179089, https://doi.org/10.1016/j.jallcom.2025.179089.
152. Ekthammathat, N.; Phuruangrat, A.; Thongtem, S.; Thongtem, T. Synthesis, characterization and antibacterial activity of $BiVO_4$ microstructure, *Russ. J. Phys. Chem.* 2018, *92*, 1036–1040, https://doi.org/10.1134/S0036024418050114
153. Sharma, R.; Uma, Singh, S.; Verma, A.; Khanuja, M. Visible light induced bactericidal and photocatalytic activity of hydrothermally synthesized $BiVO_4$ nano-octahedrals. *J. Photochem. Photobiol. B Biol.* 2016, *162*, 266-272, https://doi.org/10.1016/j.jphotobiol.2016.06.035.
154. Saleem, A.; Ahmed, T.; Ammar, M.; Zhang, H.-l.; Xu, H.-b.; Tabassum, R. Direct growth of m-$BiVO_4$@carbon fibers for highly efficient and recyclable photocatalytic and antibacterial applications. *J. Photochem. Photobiol. B Biol*. 2020, *213*, 112070, https://doi.org/10.1016/j.jphotobiol.2020.112070.
155. Iqbal, T.; Qureshi, M.T.; Shahzad, R.; Afsheen, S.; Kausar, S.; Yunus, G.; Mansha, M. S.; Aamir, L.; Munir, R.M.; El-Serehy, H.A. Khan, M.Y.; Al-Maswari, B.M. Synergistic impacts of novel tantalum doping in $BiVO_4$ for effective photocatalytic applications, antimicrobial activity, and antioxidant aspect. *Inorg. Chem. Commun.* 2024, *170*, 113365, https://doi.org/10.1016/j.inoche.2024.113365
156. Bulut, D.T. Exploring the dual role of $BiVO_4$ nanoparticles: unveiling enhanced antimicrobial efficacy and photocatalytic performance, *J. Sol-Gel Sci. Technol*. 2025, *114*, 198–222, https://doi.org/10.1007/s10971-025-06682-z
157. 156. Ganeshbabu, M.; Kannan, N.; Venkatesh, P.S.; Paulraj, G.; Jeganathan, K.; Ali, D.M. Synthesis and characterization of $BiVO_4$ nanoparticles for environmental applications, *RSC Adv.* 2020, *10*, 18315-18322, https://doi.org/10.1039/D0RA01065K.
158. Abid, H.N.; Ahmed, D.S.; Al-keisy, A.H. Constructed p-2D/n-2D BiOCl/$BiVO_4$ nanoheterostructure for photocatalytic antibacterial activity. *ECS Trans.* 2022, *107*, 2283, https://doi.org/10.1149/10701.2283ecst
159. Li, B.; Gao,X.; Qu, J.; Xiong, F.; Xuan, H.; Jin,Y.; Yuan, H. Visible-light-driven antimicrobial activity and mechanism of polydopamine-reduced graphene oxide/$BiVO_4$ composite. *Int. J. Mol. Sci*. 2022, *23*, 7712, https://doi.org/10.3390/ijms23147712.
160. Ran, J.; Chen, H.; Bai, X.; Bi, S.; Jiang, H.; Cai, G.; Cheng, D.; Wang, X. Immobilizing CuO/$BiVO_4$ nanocomposite on PDA-templated cotton fabric for visible light photocatalysis, antimicrobial activity and UV protection. *Appl. Surf. Sci.* 2019, *493*, 1167-1176, https://doi.org/10.1016/j.apsusc.2019.07.137.
161. Wang, R.; Wu, Z.; Chen, X.; Cheng, B.; Ou, W. Water purification using a $BiVO_4$/graphene oxide multifunctional hydrogel based on interfacial adsorption-enrichment and photocatalytic antibacterial activity, *Ceram. Int*. 2023, *49*, 9657-9671, https://doi.org/10.1016/j.ceramint.2022.11.137.
162. Pramila, S.; Nagaraju, G.; Mallikarjunaswamy, C.; Latha, K.C.; Chandan, S.; Ramu, R.; Rashmi, V.; Ranganatha, V.L. Green synthesis of $BiVO_4$ nanoparticles by microwave method using *Aegle Marmelos* juice as a fuel: Photocatalytic and antimicrobial study, *Anal. Chem. Lett.* 2020, *10*, 298–306, https://doi.org/10.1080/22297928.2020.1785935.

 doi:10.20944/preprints202507.0958.v1

163. Wang, L.; Han, D.; Ni, S.; Ma, W.; Wang, W.; Niu, L. Photoelectrochemical device based on Mo-doped $BiVO_4$ enables smart analysis of the global antioxidant capacity in food. *Chem. Sci.* 2015, *6*, 6632-6638, https://doi.org/10.1039/C5SC02277K.
164. Han, F.; Luo, S.; Wu, Z.; Liang, Z.; Yang, W.; Han, D.; Sun, Z.; Liu, Z.; Niu, L. A label-free photoelectrochemical sensor based on $BiVO_4$@graphene oxide hybrid for analysis of the antioxidant capacity in food. *J. Electroanal. Chem.* 2023, *946*, 117713, https://doi.org/10.1016/j.jelechem.2023.117713.
165. Li, Y.; Dai, X.; He, L.; Bu, Y. Crystal-reconstructed BiVO4 semiconductor photoelectrochemical sensor for ultra-sensitive tumor biomarker detection. *J. Mater. Chem. B* 2022, *10*, 870-879, https://doi.org/10.1039/D1TB02576G.
166. Petruleviciene, M.; Savickaja, I.; Kovger-Jarosevic, J.; Skruodiene, M.; Juodkazyte, J.; Ramanavicius, S.; Ramanavicius, A. $BiVO_4$-based photoelectrochemical sensors for the detection of diclofenac: the role of doping, electrolytes and applied potentials. *Chemosensors* 2024, *12*, 249; https://doi.org/10.3390/chemosensors12120249.
167. Wu, W.; Tan, Z.; Chen, X.; Chen, X.; Cheng, L.; Wu, H.; Li, P.; Zhang, Z. Carnation-like morphology of $BiVO_4$-7 enables sensitive photoelectrochemical determination of Cr(VI) in the food and environment. *Biosensors* 2022, *12*, 130, https://doi.org/10.3390/bios12020130.
168. Ye, C.; Xu, S.; Wu, Z.; Wang, M. $Cu_3(PO_4)_2$/$BiVO_4$ photoelectrochemical sensor for sensitive and selective determination of synthetic antioxidant propyl gallate. *Anal Bioanal Chem* 2022, *414*, 4139–4147, https://doi.org/10.1007/s00216-022-04065-9.
169. Murugan, E.; Poongan, A. A new sensitive electrochemical sensor based on $BiVO_4$/ZrO_2@graphene modified GCE for concurrent sensing of acetaminophen, phenylephrine hydrochloride and cytosine in medications and human serum samples. *Diam. Relat. Mater*. 2022, *126*, 109117, https://doi.org/10.1016/j.diamond.2022.109117.
170. Sarikaya, I.; Kaleoglu, E.; Çakar, S.; Soykan, C.; Özacar, M. An enhanced photosensitive sensor based on ITO/MWCNTs@polymercomposite@$BiVO_4$ for quercetin detection. *Biosensors* 2023, *13*, 729, https://doi.org/10.3390/bios13070729.
171. Niu, P.B.; Cao, Q.; Huang, L.; Zhou, C.H.; Ling, J.; Hu, R.; Yang, T. Wavelength-dependent photoelectrochemical sensor array based on Bi_2WO_6/TiO_2 electrospun nanoheterojunction for multiple antioxidants identification and total antioxidant capacity analysis in natural tea. *Microchem. J.* 2024, *206*, 111568, https://doi.org/10.1016/j.microc.2024.111568.
172. Zhao, Z.; Wu, Z.; Lin, X.; Han, F.; Liang, Z.; Huang, L.; Dai, M.; Han, D.; Han, L.; Niu, L. A label-free PEC aptasensor platform based on g-C_3N_4/$BiVO_4$ heterojunction for tetracycline detection in food analysis, Food Chem. 2023, *402*, 134258. https://doi: 10.1016/j.foodchem.2022.134258
173. Wang, S.; Li, C.; Yu Qi, Zhang, J.; Wang, N.; Liu, M.; Zhang, B.; Cai, X.; Zhang, H.; Wei, Su-h.; Ma, G.; Yang, J.; Chen, S.; Zhang, F. Etched $BiVO_4$ photocatalyst with charge separation efficiency exceeding 90%, *Nat Commun* 2025, *16*, 3776, https://doi.org/10.1038/s41467-025-59076-8.
174. X. Tao, Y. Zhao, S. Wang, C. Li, R. Li, Recent advances and perspectives for solar-driven water splitting using particulate photocatalysts, *Chem. Soc. Rev.* 2022, *51*, 3561-3608, https://doi.org/10.1039/D1CS01182K
175. Wang, S.; Wan, K.; Feng, J.; Yang, Y.; Wang, S. $BiVO_4$ photoanodes with enhanced photoelectrochemical performance: Preparation, modification and emerging applications, *J. Mater. Sci. Tech.* 2025, *217*, 182–220, https://doi.org/10.1016/j.jmst.2024.08.014
176. Huang, J.; Lin, T.; Lin, L.; Ma, G.; Zhang, Z.; Handschuh-Wang, S.; Meng, A.; Han, P.; He, B. Boosted charge transport efficiency for bismuth and oxygen dual vacancy-engineered $BiVO_4$ photoanodes, *ACS Appl. Energy Mater.* 2024, *7*, 10710–10720, https://doi.org/10.1021/acsaem.4c02394.
177. Liu, B.; Wang, X.; Zhang, Y.; Wan, K.; Xu, L.; Ma, S.; Zhao, R.; Wang, S.; Huang, W. Bismuth vacancies induced lattice strain in $BiVO_4$ photoanodes boosting charge separation for water oxidation, *Adv. Energy Mater.* 2025, *15*, 2403835, https://doi.org/10.1002/aenm.202403835.
178. Yi, Qinghua, Wang, H.; Lee, J.-M. $BiVO_4$-based photoelectrochemical water splitting, *ChemElectroChem* 2025, *12*, e202400600, https://doi.org/10.1002/celc.202400600.
179. Wang, Z.; Li, C.; Domen, K. Recent developments in heterogeneous photocatalysts for solar-driven overall water splitting. *Chem. Soc. Rev*. 2019, *48*, 2109–2125, https://doi.org/10.1039/C8CS00542G.

 doi:10.20944/preprints202507.0958.v1

180. Nasir, J.A.; Munir, A.; Ahmad, N.; Haq, T.; Khan, Z.; Rehman, Z. Photocatalytic Z-scheme overall water splitting: recent advances in theory and experiments, *Adv. Mater.* 2021, 33, 2105195, https://doi.org/10.1002/adma.202105195.
181. Zhou, P.; Navid, I.A.; Ma, Y.; Xiao, Y.; Wang, P.; Ye, Z.; Zhou, B.; Sun, K.; Mi, Z. Solar-to-hydrogen efficiency of more than 9% in photocatalytic water splitting, *Nature* 2023, *613*, 66-70, (https://doi.org/10.1038/s41586-022-05399-1.
182. Hwang, S.W.; Jeong Y.J.; Tan, R.; Saravanan, I.; Han, H.S.; Kim, D.H.; Cho, I.S. Texture development and surface reconstruction of $BiVO_4$ photoanode via one-pot hydrothermal reaction for enhanced photoelectrochemical water splitting, *J. Adv. Ceram.* 2025, *14*, 9221043, https://doi.org/10.26599/JAC.2025.9221043.
183. Chi, J.; Wei, Z.; Fang, W.; Yan, J.; Wang, J.; Zu. H.; Cheng, J.; Luo, H.; Ye, Z.; Liu, J.; Jiang, Z.; Shangguan, W. Octadecahedral $BiVO_4$ with exposed high-reactivity {121} facets for enhanced photoelectrochemical water splitting, *Appl. Catal., B: Environ.* 2025, *365*, 124973, https://doi.org/10.1016/j.apcatb.2024.124973.
184. Xiao, C.; Assavachin, S.; Hahn, W.; Wang, L.; van Benthem, K.; Osterloh, F.E. Flux synthesis of single crystal bismuth vanadate ($BiVO_4$) nanowires and their visible light driven photocatalytic water oxidation properties, *J. Mater. Chem. A* 2025, *13*, 7834-7844, https://doi.org/10.1039/D4TA08318K.
185. Veetil; S.P.; Vattakkoval; N.; Veedu; S.K.; Vijayan, B.K. Supercapacitor applications of cerium doped $BiVO_4$ nanosheets as electrode materials, *AIP Conf. Proc.* 2025, *3198*, 020131, https://doi.org/10.1063/5.0248453.
186. 184. Wan, X.; Luo, X.; Lu, D.; Liu, G.; Fu, Y.; Cai, L.; Hu, C.; Wan, H. Controllable fabrication of Cu: $BiVO_4$ nanostructures via a two-step electrodeposition strategy for efficient photoelectrochemical water splitting, *J. Alloys Compd.* 2025, *1010*, 177903, https://doi.org/10.1016/j.jallcom.2024.177903.
187. Wang, H.; Bai, Y.; Wang, R.; Fu, Y.; Mei, Q.; Bai, B.; Wang, Q. Boosting photoelectrochemical water splitting: enhanced hole transport in $BiVO_4$ photoanodes *via* interfacial coupling, *Catal. Sci. Technol.* 2025, *15*, 405-415, https://doi.org/10.1039/D4CY01284D.
188. Ti_3C_2 quantum dots decorated $BiVO_4$ photoelectrode for both photoelectrochemical water splitting and H_2O_2 determination, *J. Alloys Compd.* 2025, *1011*, 178399, https://doi.org/10.1016/j.jallcom.2024.178399.
189. Li, H.; Lyu, M.; Lai, Y.; Cheng, X.; Dong, Z. For effective water splitting by inserting a p-type copper thiocyanate hole transfer layer between $BiVO_4$ and Ni-doped FeOOH cocatalyst, Int. J. Hydrog. Energy 2025, *106*, 1006-1015, https://doi.org/10.1016/j.ijhydene.2025.02.043.
190. Saad, A.M.; Mady, A.H.; Sayed, M.S.; Kim, G.; Kim, M.; Kim, W.K. Boosting water oxidation kinetics of $BiVO_4$ through a metal-organic co-catalyst enriched with phosphate groups (Co,Fe-NTMP): Insights from LMCT mechanism and DFT study, *Appl. Catal. B: Environ. Energy* 2025, *370*, 125163, https://doi.org/10.1016/j.apcatb.2025.125163.
191. Kavitha, T.; Rojviroon, O.; Rajendran, R.; Rojviroon, T. Construction of hybrid 2D g-C_3N_4/$BiVO_4$ photocatalyst decorated with RGO for enhancing the H_2 production and photocatalytic degradation of antibiotics, *J. Porous Mater*. 2025, *In Press*, https://doi.org/10.1007/s10934-025-01778-x
192. Miao, Z.; Wang R.; Li, X.; Sun, F.; Ge, M.; Huang, N.; Zhao, Y.; Chang, Z.; Wang, H. Photoreduced Ag nanoparticles-decorated $BiVO_4$ nanoplates as photoanode boosting photoelectrochemical H_2O_2 fuel cell performance, *J. Power Sources* 2025, *629*, 235998, https://doi.org/10.1016/j.jpowsour.2024.235998.
193. Andrei, V.; Chiang, Y.-H.; Rahaman, M.; Anaya, M.; Kang, T.; Ruggeri, E.; Stranks, S.D.; Reisner, E. Modular perovskite-$BiVO_4$ artificial leaves towards syngas synthesis on a m^2 scale, *Energy Environ. Sci.* 2025, *18*, 3623-3632, https://doi.org/10.1039/D4EE05780E.
194. Fu, H.; Wu, Y.; Guo, Y.; Sakurai, T.; Zhang, Q.; Liu, Y.; Zheng, Z.; Cheng, H.; Wang, Z.; Huang, B.; Wang, Q.; Domen, K.; Wang, P. A scalable solar-driven photocatalytic system for separated H_2 and O_2 production from water, *Nat. Commun*. 2025, *16*, 990. https://doi.org/10.1038/s41467-025-56314-x.